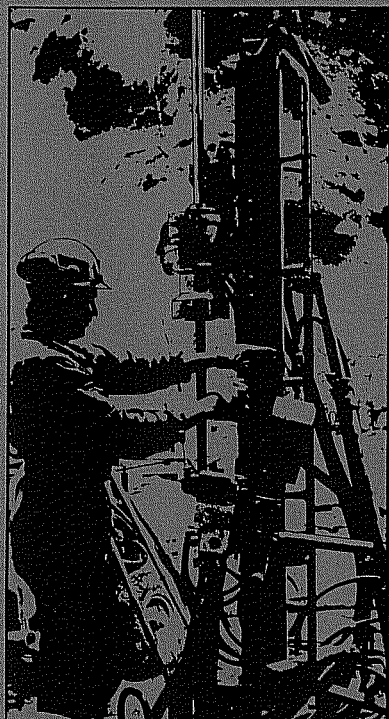


SWEDISH-AMERICAN COOPERATIVE PROGRAM ON RADIOACTIVE WASTE STORAGE IN MINED CAVERNS IN CRYSTALLINE ROCK



Technical Information Report No. 28

A LABORATORY ASSESSMENT OF THE USE OF BOREHOLE PRESSURE TRANSIENTS TO MEASURE THE PERMEABILITY OF FRACTURED ROCK MASSES

C. B. Forster and J. E. Gale

Department of Earth Sciences
University of Waterloo
Waterloo, Ontario, Canada

September 1980

A Joint Project of

Swedish Nuclear Fuel Supply Co.
Fack 10240 Stockholm, Sweden

Operated for the Swedish
Nuclear Power Utility Industry

Lawrence Berkeley Laboratory
Earth Sciences Division
University of California
Berkeley, California 94720, USA

Operated for the U.S. Department of
Energy under Contract W-7405-ENG-48

This report was prepared as an account of work sponsored by the United States Government and/or the Swedish Nuclear Fuel Supply Company. Neither the United States nor the U.S. Department of Energy, nor the Swedish Nuclear Fuel Supply Company, nor any of their employees, nor any of their contractors, subcontractors, or their employees, makes any warranty, express or implied or assumes any legal liability or responsibility for the accuracy, completeness or usefulness of any information, apparatus, product or process disclosed, or represents that its use would not infringe privately owned rights.

Printed in the United States of America
Available from
National Technical Information Service
U.S. Department of Commerce
5285 Port Royal Road
Springfield, VA 22161
Price Code: A06

This report is part of a cooperative Swedish-American project supported by the U.S. Department of Energy and/or the Swedish Nuclear Fuel Supply Company. Any conclusions or opinions expressed in this report represent solely those of the author(s) and not necessarily those of The Regents of the University of California, the Lawrence Berkeley Laboratory, the Department of Energy, or the Swedish Nuclear Fuel Supply Company.

Reference to a company or product name does not imply approval or recommendation of the product by the University of California or the U.S. Department of Energy to the exclusion of others that may be suitable.

TECHNICAL INFORMATION DEPARTMENT
LAWRENCE BERKELEY LABORATORY
UNIVERSITY OF CALIFORNIA
BERKELEY, CALIFORNIA 94720

ANDREW DUBOIS
EARTH SCIENCES DIV
BLDG 90, RM 1070D
LBL

284707

62

A LABORATORY ASSESSMENT OF THE USE OF
BOREHOLE PRESSURE TRANSIENTS TO MEASURE THE
PERMEABILITY OF FRACTURED ROCK MASSES

by

C.B. Forster
J.E. Gale

Department of Earth Sciences
University of Waterloo
Waterloo, Ontario, Canada

September, 1980

This report was prepared by the Lawrence Berkeley Laboratory under the University of California Contract W-7405-ENG-48 with the Department of Energy. Funding for this project is administered by the Office of Nuclear Waste Isolation at Battelle Memorial Institute.



PREFACE

This report is one of a series documenting the results of the Swedish-American cooperative research program in which the cooperating scientists explore the geological, geophysical, hydrological, geochemical, and structural effects anticipated from the use of a large crystalline rock mass as a geologic repository for nuclear waste. This program has been sponsored by the Swedish Nuclear Power Utilities through the Swedish Nuclear Fuel Supply Company (SKBF), and the U.S. Department of Energy (DOE) through the Lawrence Berkeley Laboratory.

The principal investigators are L.B. Nilsson and O. Degerman for SKBF, and N.G.W. Cook, P.A. Witherspoon, and J.E. Gale for LBL. Other participants will appear as authors of the individual reports.

Previous technical reports in this series are listed below.

1. Swedish-American Cooperative Program on Radioactive Waste Storage in Mined Caverns by P.A. Witherspoon and O. Degerman. (LBL-7049, SAC-01).
2. Large Scale Permeability Test of the Granite in the Stripa Mine and Thermal Conductivity Test by Lars Lundstrom and Haken Stille. (LBL-7052, SAC-02).
3. The Mechanical Properties of the Stripa Granite by Graham Swan (LBL-7074, SAC-03).
4. Stress Measurements in the Stripa Granite by Hans Carlsson (LBL-7078, SAC-04).
5. Borehole Drilling and Related Activities at the Stripa Mine by P.J. Kurfurst, T. Hugo-Persson, and G. Rudolph (LBL-7080, SAC-05).
6. A Pilot Heater Test in the Stripa Granite by Hans Carlsson (LBL-7086, SAC-06).
7. An Analysis of Measured Values for the State of Stress in the Earth's Crust by Dennis B. Jamison and Neville G.W. Cook (LBL-7071, SAC-07).
8. Mining Methods Used in the Underground Tunnels and Test Rooms at Stripa by B. Andersson and P.A. Halen (LBL-7081, SAC-08).
9. Theoretical Temperature Fields for the Stripa Heater Project by T. Chan, Neville G.W. Cook, and C.F. Tsang (LBL-7082, SAC-09).
10. Mechanical and Thermal Design Considerations for Radioactive Waste Repositories in Hard Rock. Part I: An Appraisal of Hard Rock for Potential Underground Repositories of Radioactive Waste by N.G.W. Cook; Part II: In Situ Heating Experiments in Hard Rock: Their Objectives and Design by N.G.W. Cook and P.A. Witherspoon (LBL-7073, SAC-10).
11. Full-Scale and Time-Scale Heating Experiments at Stripa: Preliminary Results by N.G.W. Cook and M. Hood (LBL-7072; SAC-11).

12. Geochemistry and Isotope Hydrology of Groundwaters in the Stripa Granite: Results and Preliminary Interpretation by P. Fritz, Barker, and J.E. Gale (LBL-8285, SAC-12).
13. Electrical Heaters for Thermo-Mechanical Tests at the Stripa Mine by R.H. Burleigh, E.P. Binnall, A.O. DuBois, D.O. Norgren, and A.R. Ortiz (LBL-7063, SAC-13).
14. Data Acquisition, Handling, and Display for the Heater Experiments at Stripa by Maurice B. McEvoy (LBL-7062, SAC-14).
15. An Approach to the Fracture Hydrology at Stripa: Preliminary Results by J.E. Gale and P.A. Witherspoon (LBL-7079, SAC-15).
16. Preliminary Report on Geophysical and Mechanical Borehole Measurements at Stripa by P. Nelson, B. Paulsson, R. Rachiele, L. Andersson, T. Schrauf, W. Hustrulid, O. Duran, and K.A. Magnussen (LBL-8280, SAC-16).
17. Observations of a Potential Size-Effect in Experimental Determination of the Hydraulic Properties of Fractures by P.A. Witherspoon, C.H. Amick, J.E. Gale, and K. Iwai (LBL-8571, SAC-17).
18. Rock Mass Characterization for Storage in Nuclear Waste in Granite by P.A. Witherspoon, P. Nelson, T. Doe, R. Thorpe, B. Paulsson, J.E. Gale, and C. Forster (LBL-8570, SAC-18).
19. Fracture Detection in Crystalline Rock Using Ultrasonic Shear Waves by K.H. Waters, S.P. Palmer, and W.F. Farrell (LBL-7051, SAC-19).
20. Characterization of Discontinuities in the Stripa Granite--Time Scale Heater Experiment by R. Thorpe (LBL-7083, SAC-20).
21. Geology and Fracture System at Stripa by A. Olkiewicz, J.E. Gale, R. Thorpe, and B. Paulsson (LBL-8907, SAC-21).
22. Calculated Thermally Induced Displacements and Stresses for Heater Experiments at Stripa by T. Chan and N.G.W. Cook (LBL-7061, SAC-22).
23. Validity of Cubic Law for Fluid Flow in a Deformable Rock Fracture by P.A. Witherspoon, J. Wang, K. Iwai and J.E. Gale (LBL-9557, SAC-23).
24. Determination of In-Situ Thermal Properties of Stripa Granite from Temperature Measurements in the Full-Scale Heater Experiments: Methods and Primary Results by J. Jeffrey, T. Chan, N.G.W. Cook and P.A. Witherspoon (LBL-8424, SAC-24).
25. Instrumentation Evaluation, Calibration, and Installation for Heater Tests Simulating Nuclear Waste In Crystalline Rock, Sweden by T. Schrauf, H. Pratt, E. Simonson, W. Hustrulid, P. Nelson, A. DuBois, E. Binnall, and R. Haught (LBL-8313, SAC-25).

26. Part I: Some Results from a Field Investigation of Thermo-Mechanical Loading of a Rock Mass When Heater Canisters are Emplaced in the Rock by M. Hood. Part II: The Application of Field Data from Heater Experiments Conducted at Stripa, Sweden for Repository Design by M. Hood, H. Carlsson, and P.H. Nelson (LBL-9392, SAC-26).
27. Progress with Field Investigations at Stripa by P.A. Witherspoon, N.G.W. Cook, and J.E. Gale (LBL-10559, SAC-27).

TABLE OF CONTENTS

	<u>Page</u>
LIST OF FIGURES	ix
LIST OF TABLES	x
NOMENCLATURE	xi
ABSTRACT	xiii
1. INTRODUCTION	1
1.1 Background	1
1.2 Objectives and Scope	5
1.3 Previous Work	6
2. THEORY OF PRESSURE PULSE TESTS	12
3. EXPERIMENTAL APPARATUS AND PROCEDURES	20
3.1 Experimental Apparatus	20
3.2 Experimental Procedures	22
3.3 Comparison of Equipment and Procedures with Theory	24
4. EXPERIMENTAL RESULTS	28
4.1 Sandstone Samples - Test Results	28
4.1.1 Steady-State Conductivity Determinations	28
4.1.2 Transient Conductivity Determinations	30
4.2 Stripa Granite Sample with a Single Fracture - Test Results	41
4.2.1 Steady-State Conductivity Determinations	41
4.2.2 Transient Conductivity Determinations	46
5. SUMMARY AND CONCLUSIONS	54
6. ACKNOWLEDGMENTS	61
7. REFERENCES	62
APPENDIX I Development of Equations to Describe Pressure Pulse Tests Performed on a Cylindrical Sample under Hydro-Static Compression	64
1.1 Porous Cylindrical Sample	64
1.2 Porous Cylindrical Sample Containing a Single Fracture	70
1.3 Modification of Upstream Boundary Conditions to Include Packer Compliance Effects in a Simulated Borehole	76

	<u>Page</u>
APPENDIX II Test Equipment and Procedures	78
II.1 Experimental Apparatus	78
II.1.1 Pressure Application and Flow Monitoring	78
II.1.2 Simulated Borehole and Borehole Seals	80
II.1.3 Hydrostatic Sample Cell	83
II.1.4 Downstream Reservoir	85
II.1.5 Data Acquisition System	85
II.2 Experimental Procedures	85
II.2.1 Equipment Calibration	85
II.2.2 Flow Measurements	90
II.2.3 Sample Preparation	91
II.2.4 Steady-State Permeability Determinations	92
II.2.5 Transient Pressure Pulse Determinations	93
APPENDIX III Sample Descriptions	96
III.1 Berea Sandstone	96
III.2 Stripa Granite	97

LIST OF FIGURES

	<u>Page</u>
1.1 Schematic of a straddle-packer system installed in a borehole	3
1.2 Pressure versus time plot of a hypothetical pressure pulse test	4
1.3 Possible effects of packer compliance on pressure versus time decay curves	7
1.4 Schematic of the test configuration used by Brace et al. (1968).	9
2.1 Schematic of the test configuration	13
2.2 Representation of borehole seal compliance	18
3.1 Schematic of experimental apparatus	21
3.2 Reservoir volumes	27
4.1 Plot of normalized pressure against log time for two sandstone samples	33
4.2 Typical plots of log of corrected normalized pressure decay against time for two sandstone samples	36
4.3 Correlation of pressure and temperature variations	40
4.4 Confining pressure against flow rate - Stripa granite	44
4.5 Stripa granite with single fracture - loading cycle #4	47
4.6 Schematic comparison of pressure versus time plots for "open" and "closed" boundary conditions	48
4.7 Typical plot of log of normalized pressure decay against time for a granite sample containing a single fracture	51
5.1 Effect of boundary conditions on system response	60
I.1 Schematic of a porous cylindrical rock sample subjected to hydrostatic compression	65
I.2 Boundary conditions for a porous cylindrical sample	69
I.3 Schematic of a porous cylindrical rock sample containing a single fracture and subjected to hydrostatic compression	72

	<u>Page</u>
I.4	Boundary conditions for a porous cylindrical sample containing a single fracture 75
II.1	Schematic of the flow monitoring and pressure application component 79
II.2	Schematic of the simulated borehole and borehole seals 81
II.3	Schematic of the hydrostatic sample cell component 84
II.4	Schematic of the downstream reservoir 86
II.5	Schematic of the data acquisition system 87
III.1	Sketch of Stripa granite sample 97

LIST OF TABLES

3.1	Minimum flow measurement accuracy 23
4.1	Test results - Berea sandstone (sample 2-B1) 31
4.2	Test results - Berea sandstone (sample 13-B2) 32
4.3	Estimation of a^2 for two sandstone samples 38
4.4	Steady-state flow tests - Stripa granite with single fracture 42
4.5	Transient test results of Cycle #4 50
4.6	Comparison of steady-state and transient test results (granite sample - Cycle #4) 53
5.1	Comparison of average steady-state and transient K determinations for sandstone samples 55
5.2	Comparison of average steady-state and open-test transient K determinations for the granite sample 56

NOMENCLATURE

Upper Case

- A = cross-section area (L^2)
C = packer compliance coefficient (M/T^2)
F = force (ML/T^2)
I = pressure gradient (dimensionless)
K = fracture stiffness (M/T^2); also hydraulic conductivity (L/T) if not subscripted
L = sample length (L)
M = mass (M)
P = pressure [$M/(LT^2)$]
S = storage (L^3)
V = volume (L^3)
W = fracture width (L)

Lower Case

- a^2 = diffusivity term (T/L^2)
b = one half the fracture aperture (L)
k = intrinsic permeability (L^2)
q = volumetric flow rate (L^3/T)
r = coordinate direction
t = time (T)
x = coordinate direction

Greek Letters

- α = negative slope of log pressure versus time plot (T⁻¹)
- β = compressibility (for water if not subscripted) (LT²/M)
- γ = weight density of fluid [M/(L²T²)]
- λ = coefficient for boundary conditions (T/L)
- ρ = mass density of fluid (M/L³)
- μ = dynamic viscosity of fluid (M/LT)

Subscripts

- C = confining; also corrected
- D = downstream
- e = due to external pressure
- eff = effective
- E = equalization
- f = fracture
- i = prior to zero time
- N = normalized
- p = porous; also piston
- R = rock
- s = solid; also at standard temperature of 15.6°C
- t = transient
- T = at test temperature T
- U = upstream
- 0 = at zero time
- 1 = upstream
- 2 = downstream
- 3 = total or confining

ABSTRACT

A laboratory program is described that was designed (1) to evaluate the degree of correlation between permeability values determined from steady-state and transient tests on the same samples and (2) to determine the effects of packer compliance on pressure pulse tests performed on low permeability rocks. The basic theory of pressure pulse testing is reviewed and modifications are proposed that may account for packer compliance effects.

The laboratory set-up simulates a full-scale field situation using standard field packers in a 76 mm steel pipe. Cylindrical samples 5 cm in diameter and 11 cm long can be subjected to hydrostatic confining pressure up to 34 MPa and pore pressures up to 10 MPa. Using this equipment, transient pressure pulse tests and steady-state flow tests have been performed on (1) two samples of Berea sandstone having conductivities of 6.1×10^{-5} cm/sec and 2.4×10^{-4} cm/sec. and (2) one sample of Stripa granite containing a single fracture parallel to the core axis. Flow through the fracture varied from 1.0 to 0.05 cm³/min when the confining pressure varied from about 3 MPa to 14 MPa for pressure differentials of 0.14 MPa.

Transient tests on the porous media samples consistently gave lower permeability values than steady-state tests on the same samples. All samples showed distinct compliance effects that increased with decreasing permeability. The laboratory results demonstrated that transient tests are very sensitive to minor leaks in the test assembly and to temperature variations as slight as $\pm 0.05^\circ\text{C}$ in the cavity fluid. Thus pressure-pulse borehole equipment must be carefully checked in full-scale test assemblies and must incorporate temperature measuring devices that can detect changes of $\pm 0.01^\circ\text{C}$.

1. INTRODUCTION

1.1 Background

Analysis of contaminant movement through low permeability fractured argillaceous and crystalline rock must be based on a detailed understanding of the physical hydrology of such rock masses. Fractured rock masses are generally characterized by narrow, relatively permeable zones within a low permeability framework. These zones are either discrete fractures, closely spaced groups of fractures or thin porous media zones. The matrix hydraulic conductivities of most argillaceous and crystalline rocks generally range from 10^{-9} cm/sec to less than 10^{-12} cm/sec. The hydraulic conductivity of the narrow, relatively permeable zones can be many orders of magnitude greater.

Because it is planned to locate repositories at depths of 1000 m or greater, single-well testing techniques are needed that can test and characterize high permeability zones over borehole intervals of one to three meters at such depths. Existing single-well testing techniques include tracer tests, falling head tests, steady state flow tests and borehole geophysical surveys. In low permeability rocks tracer and falling head tests take a long time to complete, steady state tests are limited to flowrates greater than 0.01 to 0.001 cc/min and geophysical tools are not sensitive enough to provide quantitative data in such rock masses. However, the pressure pulse technique of Brace et al. (1968) may overcome some of these limitations. This technique consists of accurately measuring small induced pressure transients (amounting to only a few percent of in-situ water pressures) over relatively short periods ranging from minutes to days. This should permit one to measure low permeabilities over short borehole intervals. Thus

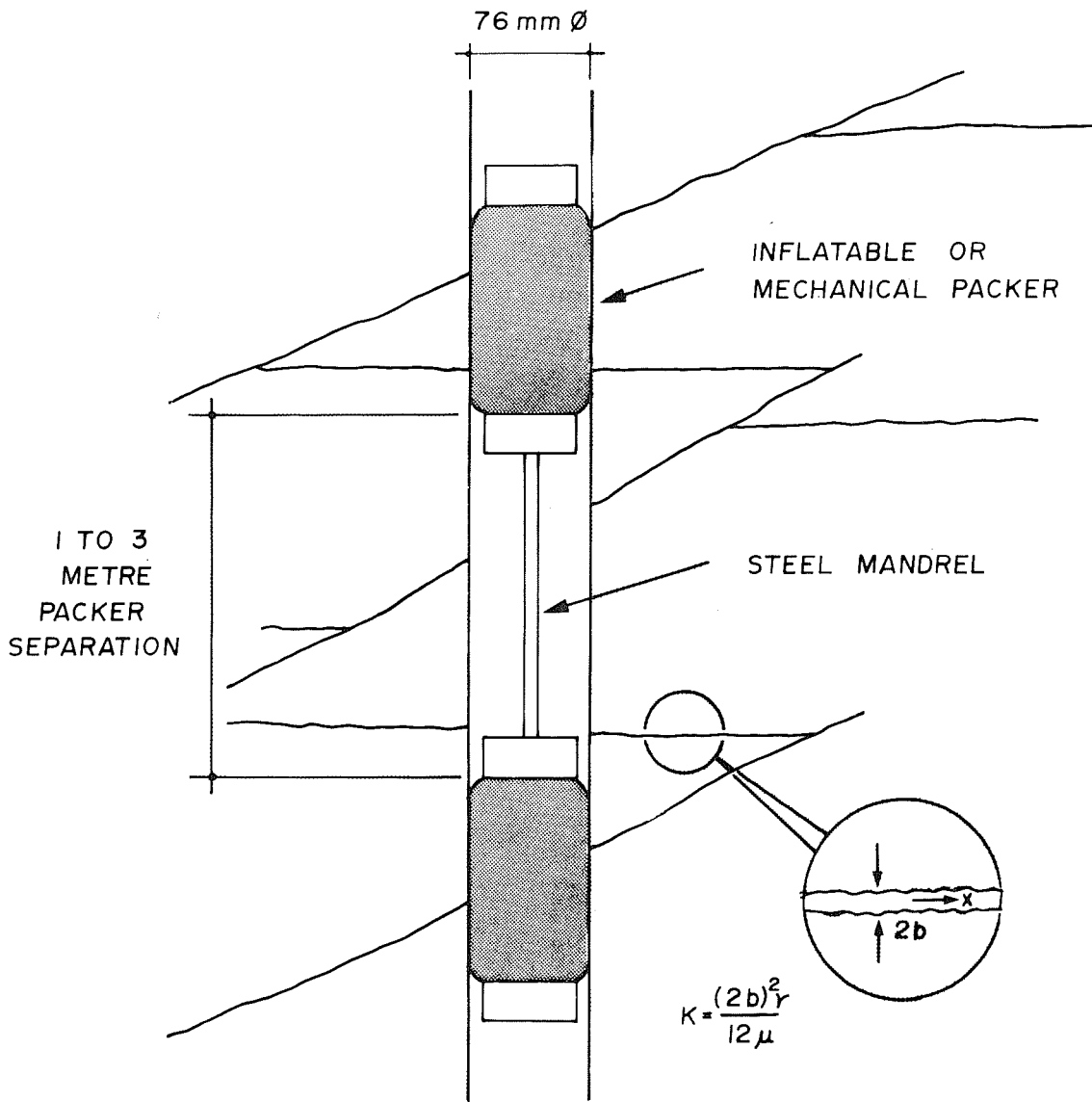
in fractured media, where even the simplest fracture systems will be difficult to understand, single fractures may be tested and overall rock mass permeabilities estimated from individual fracture characteristics (Gale, 1980; Gale and Witherspoon, 1979).

Four steps might be followed in a field pressure transient test:

1. Data from core logs, borehole TV logs, geophysical logs, and possibly injection tests (performed over long borehole intervals) are used to select the desired borehole intervals.
2. A straddle-packer system is used to isolate the specified interval (Fig. 1.1).
3. A pressure pulse is generated within the cavity and the resulting pressure decay is monitored using a sensitive electronic pressure transducer.
4. Field results may be analyzed by comparison with pressure-time data generated by numerical or analytical solutions of the diffusivity equation with appropriate boundary conditions.

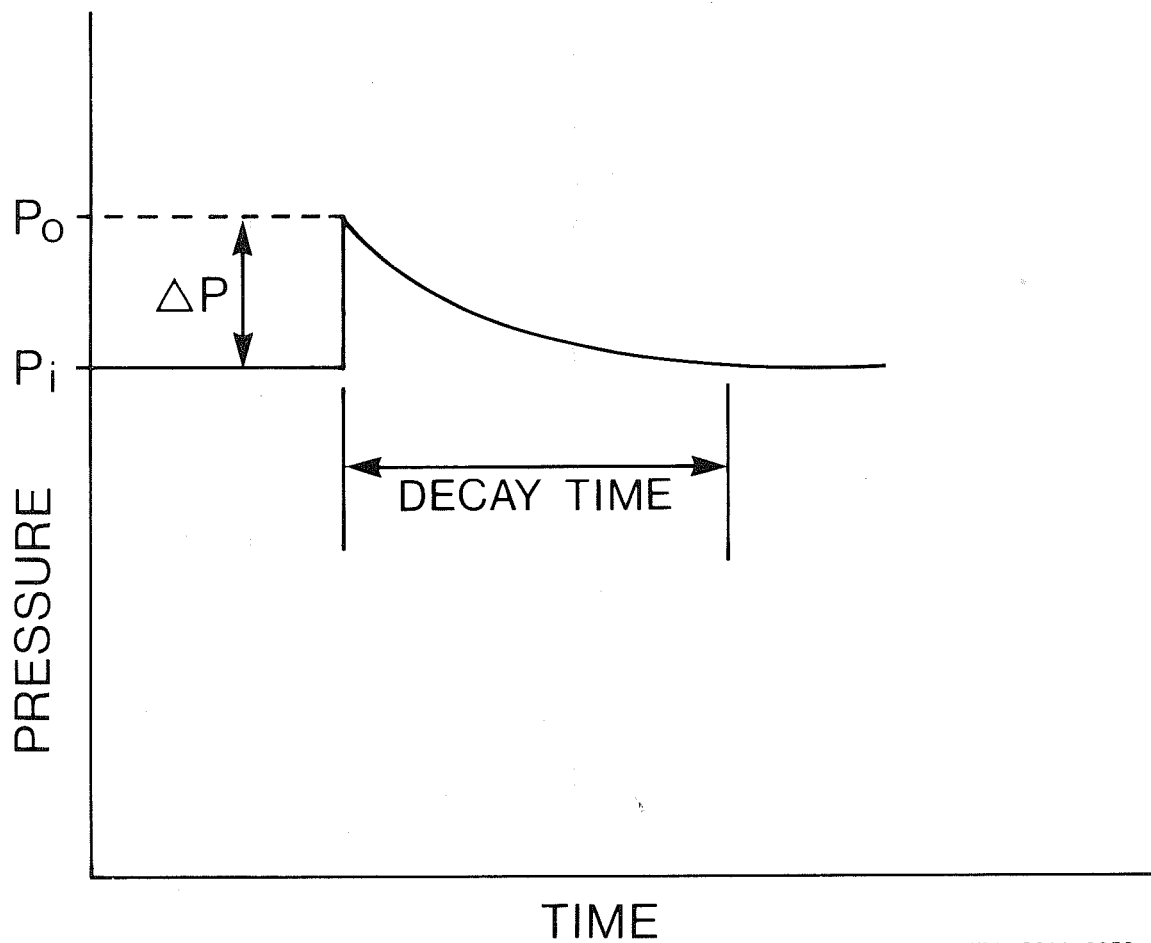
The character of the resulting pressure-time decay curve (Fig. 1.2) should correspond to a unique rock-mass conductivity for the particular borehole configuration and water and rock properties.

A basic assumption required in any attempt to analyze field data is that the borehole interval volume remains constant throughout the test. Variations in the volume of the test interval, due to packer compliance (elasticity), may mask the character of the decay curves and significantly affect the resulting conductivity determinations. Pressure pulse conductivity determinations, made in the laboratory, have not been correlated against



XBL 8011-3951

Fig. 1.1 Schematic of a straddle-packer system installed in a borehole.



XBL 8011-3952

Fig. 1.2 Pressure versus time plot of a hypothetical pressure pulse test.

standard conductivity determination techniques. Also, except for the work of Brace et al. (1968), it has not been proven that the present theory of pressure pulse tests provides accurate values of conductivity for either the field or laboratory situation.

1.2 Objectives and Scope

The objective of this study is to determine: 1) if present theory of conductivity determination by pressure pulse tests can be applied to field test data, 2) if volume changes caused by packer system compliance in the borehole cavity during testing are significant and hence 3) whether equipment and/or theory must be modified to perform and interpret pressure pulse borehole results. For background, this report reviews the basic theory of pressure pulse testing, as applied to porous media. In addition, modifications to the theory are outlined that permit one to analyze fractured samples and incorporate the effects of packer compliance in the basic equations.

A full-scale borehole is simulated by a steel pipe 7 m long and 0.076 m inside diameter. Using standard field packers, a full-scale borehole cavity, up to 3 m in length, can be isolated in the pipe. A pressure pulse generated in the cavity is transmitted to a downstream reservoir through a cylindrical rock sample. Also, standard steady-state flow tests can be carried out on the test samples. This configuration allows one to use simple one-dimensional flow theory for test analysis.

In this study, steady-state and pressure pulse tests were carried out on two samples of Berea sandstone (porous media) and a sample of the Stripa granite containing a single fracture. Hydraulic conductivity values have been calculated from both tests and the results compared for each

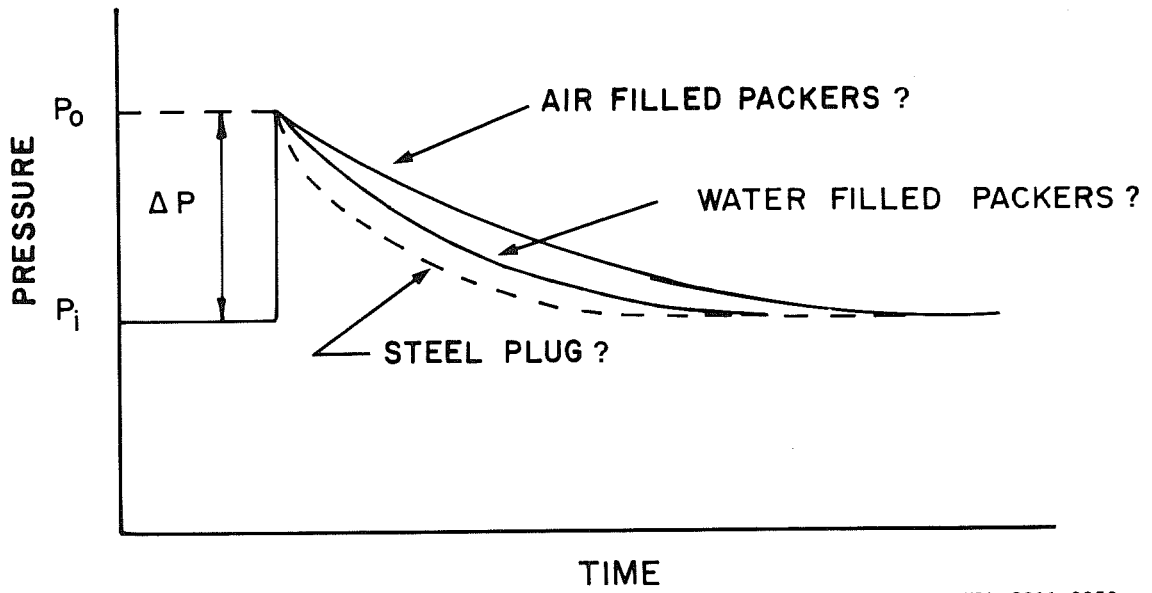
sample.

The significance of compliance effects on pressure-time decay curves (Fig. 1.3) has been investigated. A range of compliance effects have been simulated by using three types of borehole seals--air-inflated packers, water-inflated packers and a steel plug in the simulated borehole (steel pipe). The results of this work suggest that care must be exercised in performing pressure pulse tests to ensure that the test equipment and test procedures are consistent with the assumptions inherent in the basic theory.

1.3 Previous Work

The pressure pulse test bears some similarity to the falling-head test used in water resources and geotechnical investigations and holds the same name as the multiple-well test technique used in the petroleum industry. However, the method of analysis is quite different. Thus, this section reviews significant papers relating only to the pressure pulse test described herein. For descriptions of the analysis of falling head tests used in the water resources and geotechnical industries, see Hvorslev (1951), Cooper et al. (1967), Papadopoulos et al. (1973) and Bouwer and Rice (1976). The petroleum industry techniques are well reviewed by Earlougher (1977).

Methods for analysis of pressure pulse tests were first proposed by Brace et al. (1968) in work they performed on unfractured rock samples. Lin (1977) used a more complete form of their mathematical formulation in a numerical simulation of a proposed laboratory testing program. Wang et al. (1977) proposed and investigated a method for analysis of in-situ pulse tests in fractured impermeable media that uses a semi-analytical model based on solution of the diffusivity equation for different test configurations, and



XBL 8011-3953

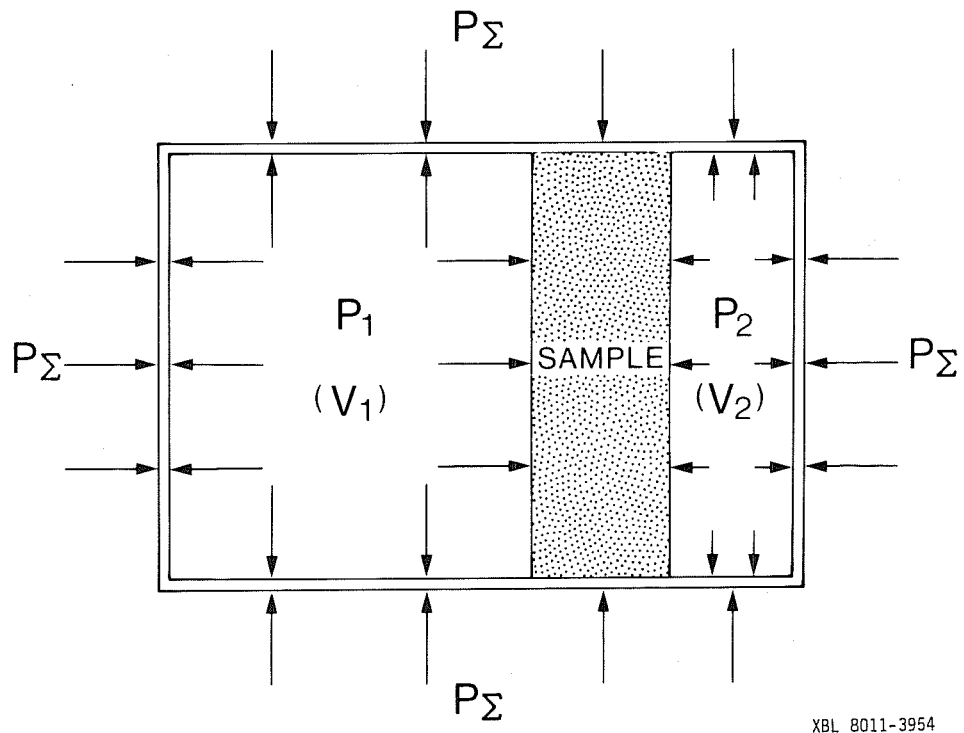
Fig. 1.3 Possible effects of packer compliance on pressure versus time decay curves.

appropriate rock and water properties and boundary conditions.

The tests of Brace et al. were conducted on small samples (length, 1.61 cm; area, 5.0 cm²) of unfractured Westerly granite subjected to relatively high confining pressures (125 to 144 MPa) using the configuration of Fig. 1.4. In their analysis, Brace and coworkers assumed that the samples were both homogeneous and isotropic and that Darcy's law was valid.

In addition, water properties (compressibility and viscosity) were assumed to be constant. This assumption required that pressure pulses be small in magnitude and temperature variations minimal during the test. Permeability values were calculated assuming a pressure gradient that is constant along the sample length and that decays exponentially to zero. This assumption is based on a rock porosity approximately equal to zero and rock compressibility much less than that of the water compressibility.

Lin used analytical and numerical techniques to investigate the effects of variations in fluid reservoir volumes in order to optimize test times for a particular sample size using the configuration and basic assumptions of Brace et al. However, due to 660-fold increase in sample size, Brace's assumption of a constant gradient was considered incorrect. Thus Lin used the complete differential equation in his analysis to compute a series of pressure-versus-time decay curves for various combinations of rock permeabilities and reservoir volumes. Pore pressures of 28 MPa and pulses (ΔP) of 2 MPa were used. The resulting data were interpreted to determine the optimum reservoir volumes for a two-reservoir test configuration.



XBL 8011-3954

Fig. 1.4 Schematic of the test configuration used by Brace et al. (1968).

Lin also investigated three techniques of equalizing, after a test, the fluid pressure within samples to pre-test values in order to determine the waiting time required between two tests. These techniques are:

1. Relaxation:

- fluid pressure in the reservoirs at each end of the sample is returned to the initial, pre-pulse, pore pressure
- a permeability of 1 nD required 11 hours for complete equalization.

2. Equalization process:

- a two cycle method of pressure reduction and increase varied above and below the initial pore pressure.
- a permeability of 1 nD required 2.8 hours for complete equalization.

3. Release of confining pressure:

- a decrease in confining pressure, in many cases, will cause an increase in sample permeability and therefore a shorter equalization time is required.

Lin concluded that a combination of method 3 with either methods 1 or 2 could be used to minimize pressure equalization times.

Wang et al. (1977) used a semi-analytical model to compute type curve solutions for tests performed in borehole intervals that intersected single or multiple fractures. Type curves were computed for fractures of finite or infinite extent and of variable aperture. Wang and coworkers assumed i) continuity of flow velocities at the wellbore fracture interface and ii) either closed (zero pressure gradient) or open (zero pressure) fractures at some distance from the well. Their initial conditions required that

the fluid pressure throughout the fracture equal the ambient pressure and that the fluid pressure in the wellbore be elevated above ambient by the magnitude of the pressure pulse at zero time. Additional assumptions in their solution were: i) the rock matrix is impermeable, therefore there is only fracture flow, ii) the laminar, parallel-plate flow law is valid, iii) water properties (compressibility and viscosity) are independent of small variations in pressure and temperature, iv) fracture aperture and test cavity dimensions are independent of small variations in pressure and v) pressure increase is instantaneous at zero time. Wang et al. concluded that since there were no variations in early-time data, despite variations in fracture volumes and boundary conditions, fracture apertures could be estimated from the decay time. Conversely the later time data provides information as to the character of fracture boundaries and permeability. However, they also point out that the resulting type curves are somewhat insensitive to the number and orientation of fractures. This renders data analysis potentially difficult unless a detailed knowledge of the fracture system to be tested is obtained or only a single fracture is tested.

In the papers discussed above, the authors assume that there are no volume change effects in the test cavity (upstream reservoir in the laboratory configuration). This is not unreasonable in the studies of Brace et al., as they utilized small reservoir volumes fabricated of steel. Compliance effects were not mentioned in discussions of the numerical pulse test simulations of Lin. Wang et al. suggest that packer compliance in the field test configuration might cause significant volume change effects within the test cavity; however, these effects were not included in their analyses.

2. THEORY OF PRESSURE PULSE TESTS

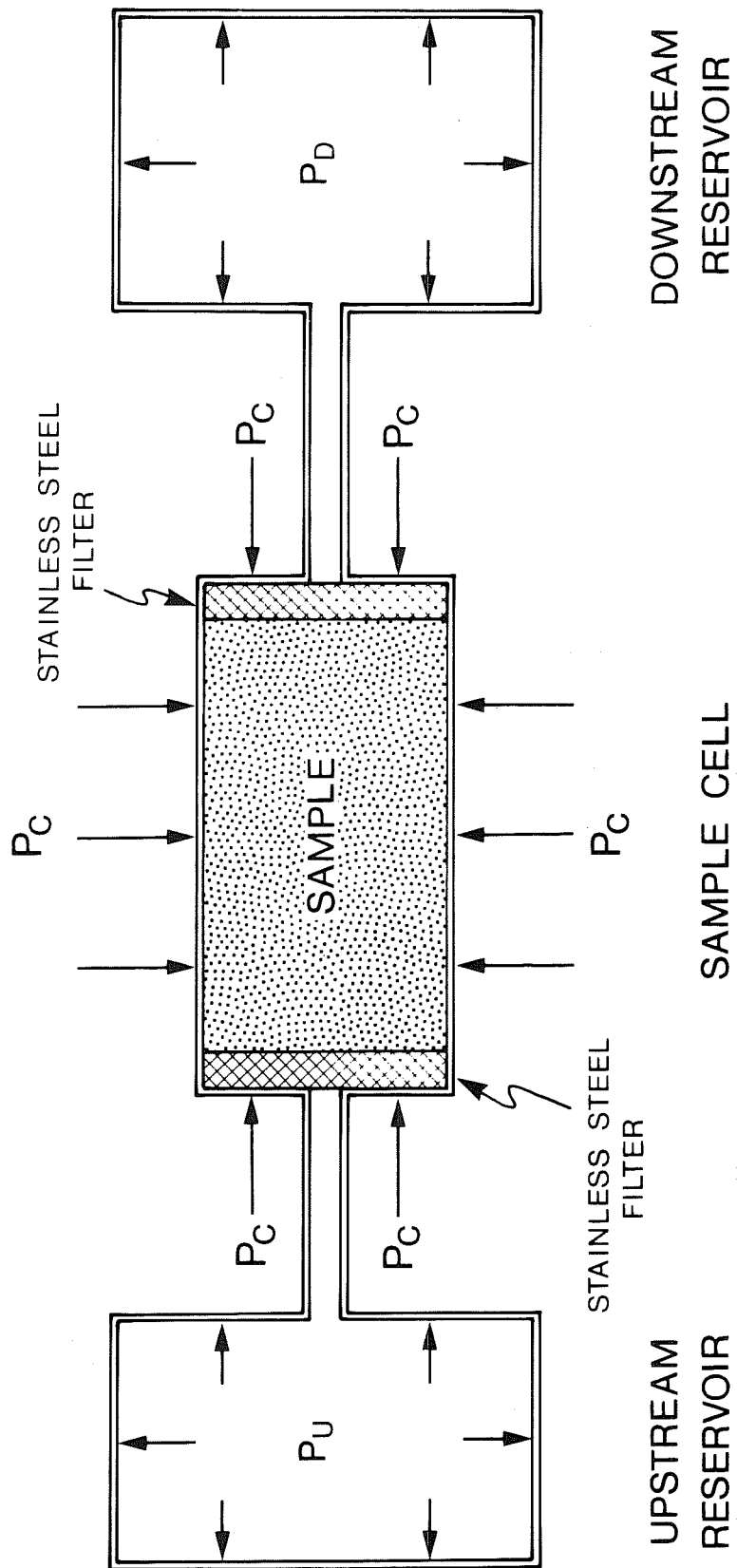
The theoretical principles of pressure pulse testing are briefly described in this chapter with particular reference to laboratory tests performed on cylindrical samples. These basic principles are used in developing the equation describing pulse tests performed on unfractured porous samples and on samples containing a single fracture. Both compliant and noncompliant boundary conditions are considered. A more detailed development of the equation presented in this chapter can be found in Appendix I.

A pressure pulse test is performed on a cylindrical rock sample under hydrostatic compression (P_C) by instantaneously increasing the pressure in one of two fluid reservoirs separated by a rock sample (Fig. 2.1). The gradient imposed across the sample causes a small volume of fluid to flow through the rock, thus equalizing the pressure in both reservoirs. The pressure decay characteristics are controlled by three rock properties -- permeability (k), porosity (n), and compressibility (β) -- and by the appropriate boundary conditions.

As a small volume of fluid flows through the sample, the fluid volume (V) in the upstream reservoir decreases. In a porous unfractured sample, flow (q) in direction x is governed by Darcy's law

$$q = \frac{dV}{dt} = \frac{-Ak}{\mu} \cdot \frac{dP}{dx} \quad (2.1)$$

where μ = dynamic fluid viscosity, k = sample permeability, dp = pressure difference across the sample, A = cross-sectional area of sample, and dx = sample length. In addition, in a low permeability sample containing a single fracture, flow through the fracture is governed by the parallel-plate, laminar



XBL 8011-3955

Fig. 2.1 Schematic of the test configuration.

flow law,

$$q = \frac{dV}{dt} = \frac{-w2bk_f}{\mu} \cdot \frac{dP}{dx} , \quad \text{where } k_f = \frac{(2b)^2}{12} . \quad (2.2)$$

here k_f = fracture permeability, $2b$ = fracture aperture, w = fracture width and 12 is a constant of integration.

The decrease in fluid volume in the upstream reservoir causes a small decrease in pressure (dP) in the reservoir. This pressure change is controlled by fluid compressibility β according to the relation

$$dP = - \frac{1}{\beta} \cdot \frac{dV}{V} . \quad (2.3)$$

In Appendix I the above constitutive relationships are combined with appropriate boundary conditions and assumptions to develop expressions for the decay of a pressure pulse, generated in the upstream reservoir as a function of time.

The equations of continuity developed in Appendix I have the form of the linear parabolic diffusivity equation

$$\frac{\partial^2 P}{\partial x^2} = a^2 \frac{\partial P}{\partial t} , \quad (2.4)$$

which describes the one-dimensional flow of a compressible fluid through a compressible porous medium. The diffusivity term, a^2 , is a function of fluid properties (compressibility and viscosity) and rock properties (compressibility, porosity and permeability). From Appendix I the a^2 term developed for an unfractured porous medium has the form

$$a^2 = \frac{\mu}{k} [-\beta_s(1 + n) + \beta_{eff} + \beta n] , \quad (2.5)$$

where μ = fluid viscosity,
 β = fluid compressibility,
 β_{eff} = effective compressibility of a jacketed sample,
 β_s = compressibility of solid grains,
 k = permeability,
 n = porosity.

The first two terms in the closed brackets represent fluid storage due to compression of the solid medium while the third term represents fluid storage due to compression of the pore fluid. Similarly, the a^2 term for a sample containing a single fracture parallel to the core axis has the form

$$a^2 = \frac{\mu}{k_f} \left[\frac{4L}{\pi K_n} + \beta(n_f + n) - \beta_s(n + 1) + \beta_{eff} \right], \quad (2.6)$$

where k_f = fracture permeability = $\frac{(2b)^2}{12}$,

L = sample length,

n_f = fracture porosity,

K_n = fracture stiffness = $\frac{dF}{d(2b)}$ = ratio of the change in outward normal force to the change in fracture aperture.

However, in addition to the components of Eq. (2.5), the effect of fluid compression in the fracture is considered, including the initial fracture porosity n_f and the variation in fracture porosity. Variation in fracture porosity is caused by variation in aperture (governed by fracture stiffness K_n) resulting from variations in fluid pressure in the fracture.

Boundary conditions developed in Appendix I have the form

$$\frac{\partial P_s}{\partial x} = \lambda \frac{\partial P_u}{\partial t} \quad (2.7)$$

Thus the change in the upstream reservoir fluid pressure P_u with time is a function of the pressure gradient in the sample $(\frac{dP_s}{dx})$ and λ where λ is a function of fluid viscosity, fluid compressibility, rock permeability (single fracture or porous media), cross section area of the sample, volume of reservoir under consideration, reservoir area and reservoir compliance.

In considering a non-compliant reservoir, for the porous media, the λ term is

$$\lambda_U = \frac{\mu V_U \beta}{kA} \quad \text{and} \quad \lambda_D = \frac{-\mu V_D \beta}{kA} \quad (2.8)$$

and the single fracture sample λ term is

$$\lambda_U = \frac{\mu V_U \beta}{k_f W 2b} \quad \text{and} \quad \lambda_D = \frac{-\mu V_D \beta}{k_f W 2b} \quad (2.9)$$

where

μ = fluid dynamic viscosity

β = fluid compressibility

V_U = upstream reservoir volume

V_D = downstream reservoir volume

k = porous media permeability

k_f = single fracture permeability = $\frac{(2b)^2}{12}$

W = fracture width

$2b$ = fracture aperture

A = cross section area of the sample

When considering a compliant upstream reservoir, a simple reservoir compliance can be simulated by a piston attached to a spring (Fig. 2.2) with the spring constant C representing the compliance term.

Thus λ has the form

$$\lambda = \frac{\mu}{kA} \left(\beta V_u + \frac{A_p^2}{C} \right) \text{ for a porous sample} \quad (2.10)$$

or

$$\lambda = \frac{\mu}{k_f W 2b} \left(\beta V_u + \frac{A_p^2}{C} \right) \text{ for a single fracture sample} \quad (2.11)$$

where A_p is the cross section area of the piston simulating reservoir compliance and C is the compliance term.

Equations (2.10) and (2.11) provide for a change in the volume of the upstream reservoir due to packer movement in the borehole. The compliance term is difficult to define analytically as the magnitude and relative effects of the compliance of various packer components are poorly known.

The initial conditions require an initial fluid pressure of P_0 in the upstream reservoir at time zero and an initial fluid pressure of P_i throughout the sample and downstream reservoir where P_0 is elevated by a pressure pulse ΔP above P_i . Thus

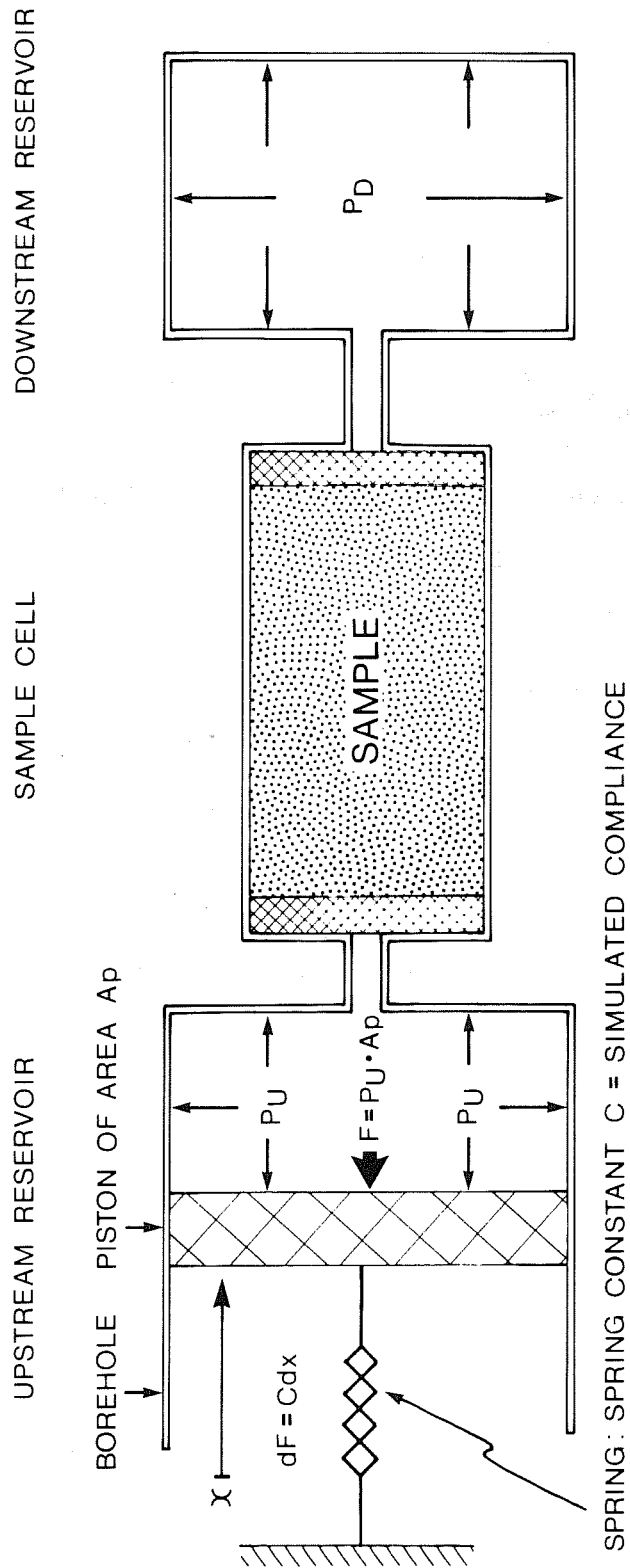
$$P(0,0) = P_0 \quad \text{and} \quad P(x,0) = P_i \quad \text{for} \quad 0 < x \leq L$$

where $P_0 = P_i + \Delta P$.

The final conditions require a pressure equalization (P_E) governed by the ratio of the upstream reservoir volume to the total system volume.

Thus

$$P(x, \infty) = P_i + \frac{\Delta P V_U}{V_U + V_D + nV_R} = P_E \quad (2.12)$$



XBL 8011-3956

Fig. 2.2 Representation of borehole seal compliance.

In developing the above equations, the main assumptions used were:

- 1) Rock sample is homogenous, isotropic and unfractured

or

Rock sample is relatively impermeable containing a continuous single fracture parallel to and centered on the core axis.

- 2) Fluid and rock properties are constant throughout the test.
- 3) Sample dimensions are constant.
- 4) The application of the pressure pulse is instantaneous.
- 5) Upstream and downstream reservoir dimensions are constant (non-compliant)

or

Upstream reservoir is compliant and compliance may be represented by a spring controlling the movement of a piston in the reservoir.

The theory developed in this chapter and in Appendix I serves to illustrate the factors involved in pressure pulse tests and will form the basis for future extensions of this work.

3. EXPERIMENTAL APPARATUS AND PROCEDURES

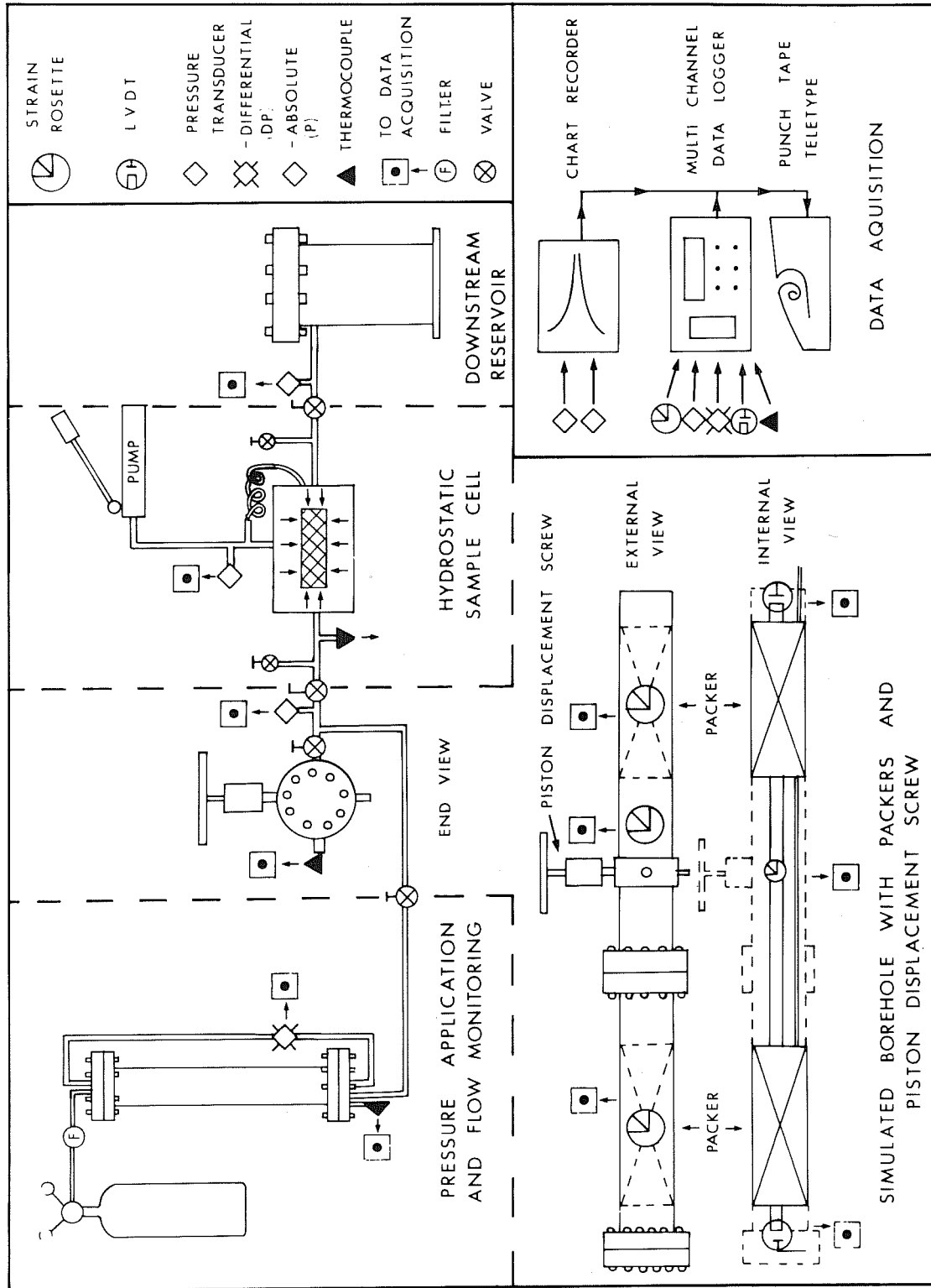
This chapter presents a brief description of the test equipment and test procedures used in this laboratory study. Equipment and procedures were designed to provide test results that could be analyzed using the theory and assumptions of Chapter 2. The first section outlines the test equipment and procedures used in steady-state and transient permeability determinations while the second illustrates the correspondence between the theoretical assumptions of Chapter 2 and the actual test set-up. Detailed discussions of the test equipment and procedures are presented in Appendix II.

3.1 Experimental Apparatus

The equipment used in this study was designed and fabricated to enable steady-state and pressure pulse permeability determinations of cylindrical samples in a configuration which could simulate a compliant or non-compliant field situation. The test configuration consists of the following five main components (Fig. 3.1):

1. Pressure application and flow monitoring
2. Simulated borehole and borehole seals
3. Hydrostatic pressure cell
4. Downstream reservoir
5. Data acquisition system

This set-up corresponds to the theoretical test configuration shown in the schematic of Fig. 2.1. A pressure pulse is generated (using the piston displacement screw) in the simulated borehole (upstream reservoir) and transmitted through the sample to the downstream reservoir. The simulated borehole is a steel tube which can represent a compliant or non-compliant upstream reservoir depending upon the type of borehole seal employed. The



XBL 8011-3957

Fig. 3.1 Schematic of experimental apparatus.

downstream reservoir is a steel tube assembled to be non-compliant at the pressures under consideration. Filter plates at each end of the sample provide an even fluid pressure distribution across the entire sample area while also transmitting the axial load to the sample ends. A urethane sleeve inside the cell transmits the radial load to the sample, which is thus subjected to hydrostatic compression. Fluid flow from the upstream to downstream reservoir is unidirectional and parallel to the core axis. During each test, thermocouples and pressure transducers at various points in the system monitor fluid pressures and temperatures, while strain gauges monitor elastic deformation of the equipment. Signal data are read using the multi-channel data logger and presented on chart records and on printed and punched teletype output.

3.2 Experimental Procedures

Experimental procedures include sample preparation, equipment calibration and performance of steady-state and transient permeability tests.

Samples were cored, cut to length and prepared (as described in Appendix II) so as to have smooth and parallel ends ensuring an even axial loading of the sample.

Thermocouples, pressure gauges, and flow measurement devices are calibrated using the techniques described in Appendix II. Thermocouples were found to provide absolute temperature measurements to $\pm 0.1^{\circ}\text{C}$ and differential temperature measurements to $\pm 0.05^{\circ}\text{C}$. Pressure transducers were calibrated against Heise gauges or a dead weight tester. Variations in fluid pressures and packer pressures of $0.0034 \text{ MPa} \pm 0.5\%$ can be resolved using the Shaevitz 0 to 3.4 MPa transducers or the Shaevitz 0 to 6.9 MPa transducers.

Variations in the hydrostatic cell pressure of 0.34 MPa may be accurately detected with the Norwood (0 to 52 MPa) transducer. Flow measurements are conducted using one of two flow tanks or a calibrated bubble line (the velocity of an air bubble moving to the outlet tube is measured and flow rates calculated).

Table 3.1 indicates the minimum flow rates that may be accurately determined, depending on the desired measurement period and measurement technique.

Table 3.1. Minimum flow measurement accuracy.

<u>Technique</u>	<u>30 minute flow</u>	<u>1 minute flow</u>
Large tank	17.7 ml/min	532 ml/min
Small tank	4.1 ml/min	122 ml/min
Bubble line	0.05 ml/min	1.6 ml/min

Steady-state permeability tests are conducted by measuring the constant rate of fluid flow through the sample due to a constant specified pressure gradient. Pressures are monitored using the transducers above and below the sample cell while flow rates are measured using one of the two flow tanks or the bubble line. Conductivity values are calculated from the test results with the aid of Darcy's law and the fluid properties at the measured test temperatures.

Transient pressure pulse determinations are performed by generating a pressure pulse (using the piston displacement screw) upstream of the sample cell, opening the intervening valve, and then allowing the pulse to be transmitted through the sample. Conductivity values are calculated from the

test results with the aid of the straight line technique of Brace et al. (1968), using the fluid properties at the measured test temperature.

3.3 Comparison of Equipment and Procedures with Theory

Data obtained from the equipment and procedures described in this chapter and Appendix II were analyzed using a simplified form of the theory presented in Chapter 2. Thus the characteristics of the test procedures and equipment must match the assumptions on which the theory is based.

Two assumptions concern characteristics of the sample rather than the equipment. The first assumption is that the sample either is homogeneous, isotropic and unfractured or contains a single continuous fracture parallel to the core axis. Samples containing a single fracture are assumed to allow negligible volumes of fluid flow through the rock matrix compared to the volume of fluid flow through the fracture. Samples used in this study were chosen to fit the above assumptions as closely as possible. The second assumption is that the sample volume remains constant. For unfractured samples, strains caused by sample compression (due to application of the pressure pulse) will yield negligible changes in the diameter or length of the sample. For fractured samples the above is considered to be true but, in addition, the change in fracture aperture (relative to the core diameter) is considered to be negligible during each test. Throughout each pulse test the sample confining pressure (P_C) is kept constant, so that variations in sample dimensions due to the pressure pulse are negligible compared with the original dimensions.

The next assumption requires verification that fluid properties are insensitive to the temperature and pressure variations encountered during

each test. Using data from Weast (1975), it can be shown that temperature variations of 0.2°C will cause the following percentage variations in water properties at room temperature (24°C):

- i) water viscosity - 0.4%
- ii) water density - $<0.01\%$
- iii) water compressibility - 0.05%

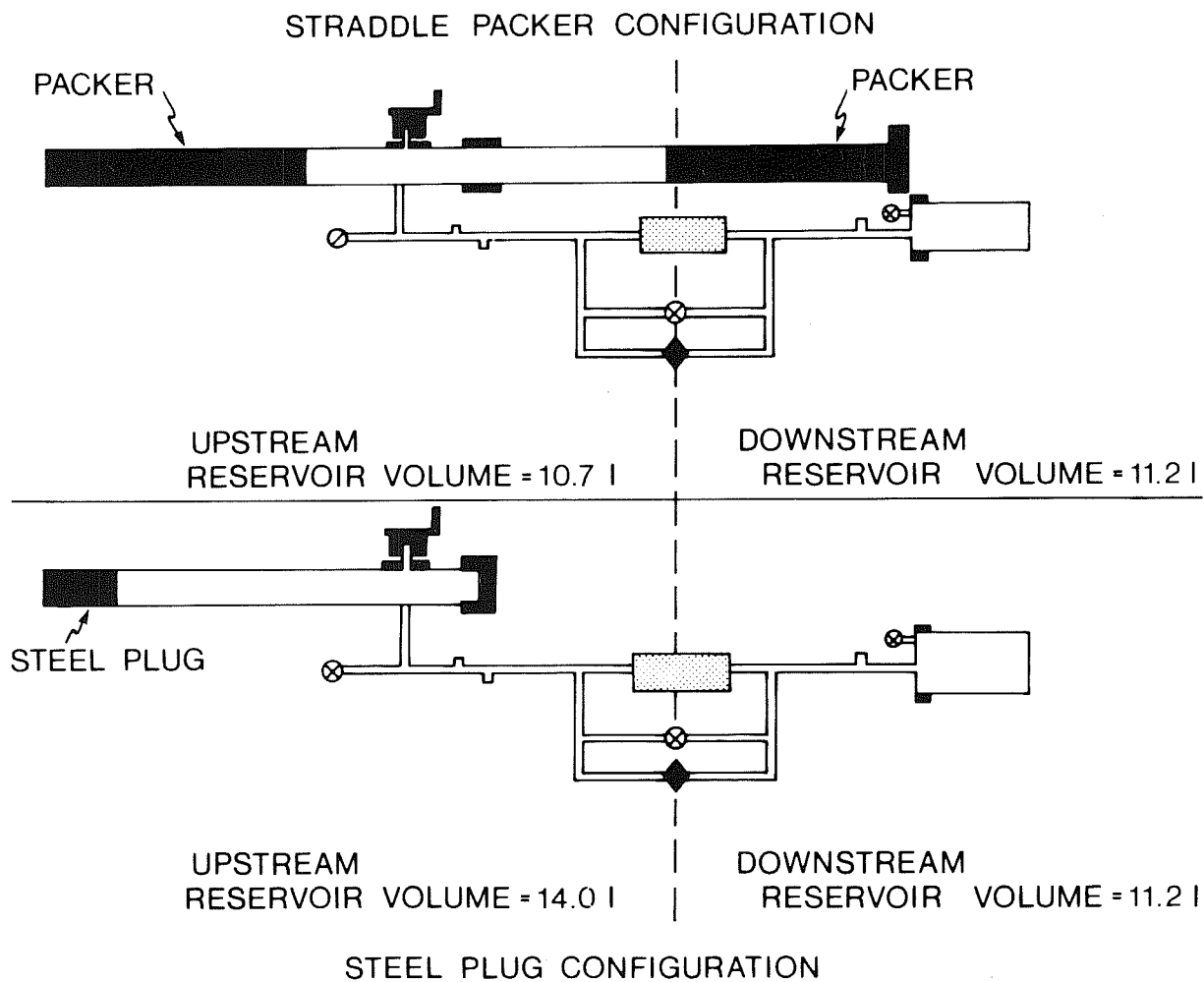
Thus if temperature variations can be maintained at less than 0.2°C , variation in water properties due to temperature change can be considered negligible. Temperature variations of 0.1°C are monitored using type T thermocouples that can resolve 0.1°C variations. Using data from Bridgman (1958) and Clarke (1966) it can also be shown that a pressure variation of 0.3 MPa will cause the following percentage variations in water properties at constant temperature (25°C):

- i) water viscosity - 0.2%
- ii) water density - 0.01%
- iii) water compressibility 0.3%

The maximum pressure variation during a single test is less than 0.3 MPa; thus variations in water properties will be negligible.

A further assumption requires an instantaneous application of the pressure pulse. This is achieved (as described in the preceding section) by generating the pressure pulse in the upstream reservoir, then allowing the pulse to decay through the sample by opening the ball valve. Opening the valve requires only a fraction of a second; thus, for decay times greater than a few seconds, the pulse application is expected to be instantaneous.

The final assumption requires non-compliant reservoirs (disregarding borehole seal compliance). Reservoir volumes are calculated from measurement of the internal dimensions of all components contributing to a specified reservoir (Fig. 3.1). Because of the large total volumes in each reservoir (about 11 liters), this somewhat rough calculation appears to yield a maximum error of measurement of approximately ± 0.01 l for an overall error of less than 0.1%. The downstream reservoir is considered to be a constant 11.2 l while the upstream reservoir holds 14.0 l in the steel plug configuration and 10.7 l in the straddle or double packer configuration (Fig. 3.2). Calculations of compliance of the steel borehole and downstream reservoir suggest volume changes of approximately 0.25 cc both upstream and downstream for pressure variations of 0.3 MPa. Thermal strains caused by a temperature change of 1°C are in the same order of magnitude as the strains caused by a 0.3 MPa pressure change (data from Hodgen et al., 1967). Thus volume changes caused by bar expansion or contraction due to pressure or temperature variations during sample testing are negligible. The strain gauge attached to the rock can be used to verify this prediction.



XBL 8011-3958

Fig. 3.2 Reservoir volumes.

4. EXPERIMENTAL RESULTS

This chapter discusses the results of steady-state and transient permeability tests performed on i) two relatively permeable and porous samples (medium to fine-grained Berea sandstone) and ii) one relatively impermeable sample (Stripa granite) containing a single natural fracture parallel to the core axis. The permeabilities of the two sandstone samples were reported to differ by one order of magnitude. The natural fracture in the granite was closed and partially healed but reopened by wedging prior to testing. Various fracture conductivities were obtained by applying several different confining pressures to the sample, thus varying the fracture aperture. More complete sample descriptions are presented in Appendix III.

Results of tests performed on the sandstone samples were reduced and analyzed prior to performing tests on the fractured granite samples. Thus observations made during testing of the sandstone were used to assist in developing modifications to equipment and procedures which were required prior to testing the lower permeability granite samples.

4.1 Sandstone Samples - Test Results

4.1.1 Steady-State Conductivity Determinations

The results of 7 steady-state conductivity tests (4 tests on sample 2-B1 and 3 tests on sample 13-B2) have been reduced and the resulting conductivity values are shown in Tables 4.1 and 4.2. With one exception, all were performed at confining pressures of 33 to 35 MPa to remove the potential for conductivity variations resulting from changes in fluid pressure (P_p) and confining pressure (P_c). Various pressure differentials ($dP = 0.13$ to 3.05 MPa) were applied across the samples (with downstream pressure approximately

Table 4.1. Test Results - Berea sandstone (sample 2-B1).

Steady state tests							Transient tests			
Test No.	P _C (MPa)	dP (MPa)	q (cc/sec)	K _{pss} (cm/sec)x10 ⁴	Test No.	ΔP (MPa)	P _C (MPa)	α ₁₀ (sec ⁻¹)	K _{pT} (cm/sec)x10 ⁴	
2-F-1	34.6	3.15	17.82	2.3	2-T _{PA} -1	0.27	31.7	0.885	2.2	
2-F-2	34.5	1.99	10.9	2.2	2-T _{PA} -2	0.17	31.7	0.885	2.2	
2-F-3	34.5	0.37	2.36	2.6	2-T _{PA} -3	0.20	31.6	0.962	2.4	
2-F-4	34.4	1.04	6.36	2.5	2-T _{PA} -4	0.27	31.9	0.967	2.4	
					2-T _{PW} -1	0.07	32.3	1.075	2.7	
					2-T _{PW} -2	0.14	32.2	1.075	2.7	
					2-T _{PW} -3	0.21	32.0	1.075	2.7	
					2-T _{PW} -4	0.28	32.5	1.000	2.5	
					2-T-1	0.27	34.5	1.075	3.1	
					2-T-2	0.26	34.5	1.053	3.0	
					2-T-3	0.27	34.0	1.087	3.1	

Note: Borehole seal designations (transient tests)

T_{PW} = Water-filled packers @ 3.4 MPa

T_{PA} = Air-filled packers @ 3.4 MPa

T = Steel plug

Table 4.2. Test results - Berea sandstone (sample 13-B2).

Steady state tests							Transient tests			
Test No.	P_C (MPa)	dP (MPa)	q (cc/sec)	K_{pss} (cm/sec)x10 ⁵	Test No.	ΔP (MPa)	P_C (MPa)	σ_{10} (sec ⁻¹)	K_{pt} (cm/sec)x10 ⁴	
13-F-1	33.0	0.31	0.408	5.5	13-T-1	0.07	34.5	0.2083	5.2	
13-F-2	32.9	0.13	0.193	6.4	13-T-3	0.14	34.5	0.2247	6.4	
13-F-3	12.9	0.30	0.466	6.4	13-T-3	0.28	34.5	0.2551	7.2	
					13-T-4	0.28	34.5	0.2394	6.8	
					13-T-5	0.14	34.5	0.2247	6.4	
					13-T-6	0.07	34.5	0.1835	4.6	
<p>Note: Borehole seal designations (transient tests) T_{PW} = Water-filled packers @ 3.4 MPa T_{PA} = Air-filled packers @ 3.5 MPa T = Steel plug</p>										
					13-T _{PA} -1	0.07	34.5	0.1117	2.8	
					13-T _{PA} -2	0.10	34.5	0.1117	2.8	
					13-T _{PA} -3	0.28	34.5	0.1025	2.6	
					13-T _{PA} -4	0.28	34.5	0.0781	1.9	
					13-T _{PW} -1	0.07	34.5	0.1398	3.5	
					13-T _{PW} -2	0.14	34.5	0.1398	3.5	
					13-T _{PW} -4	0.28	34.5	0.1398	3.5	
					13-T _{PW} -5	0.07	34.5	0.1398	3.5	
					13-T _{PW} -6	0.14	34.5	0.1453	3.6	
					13-T _{PW} -7	0.28	34.5	0.1453	3.6	

equal to zero in all tests) to determine if variations in pressure gradient result in significant conductivity variation. This information is required to compare steady-state conductivity values with conductivity determinations derived from transient tests performed at different pulse pressures. Steady-state flow tests were run for at least 15-20 minutes to ensure that steady-state conditions were achieved.

Steady-state conductivity (K_{pss}) values were calculated using sample dimensions, measured parameters and Darcy's law, where

$$q = \frac{-k\gamma_T A}{\mu_T} \frac{dh}{dx} \quad , \quad (4.1)$$

$$K_{pss} = \frac{k\gamma_S}{\mu_S} = -q \frac{\gamma_S}{\gamma_T} \cdot \frac{dx}{dh} \cdot \frac{1}{A} \cdot \frac{\mu_T}{\mu_S} \quad . \quad (4.2)$$

Here, dx = sample length (cm),

A = sample cross-section area (cm²),

q = volume flow rate calculated from measured fluid displacement (cm³/sec),

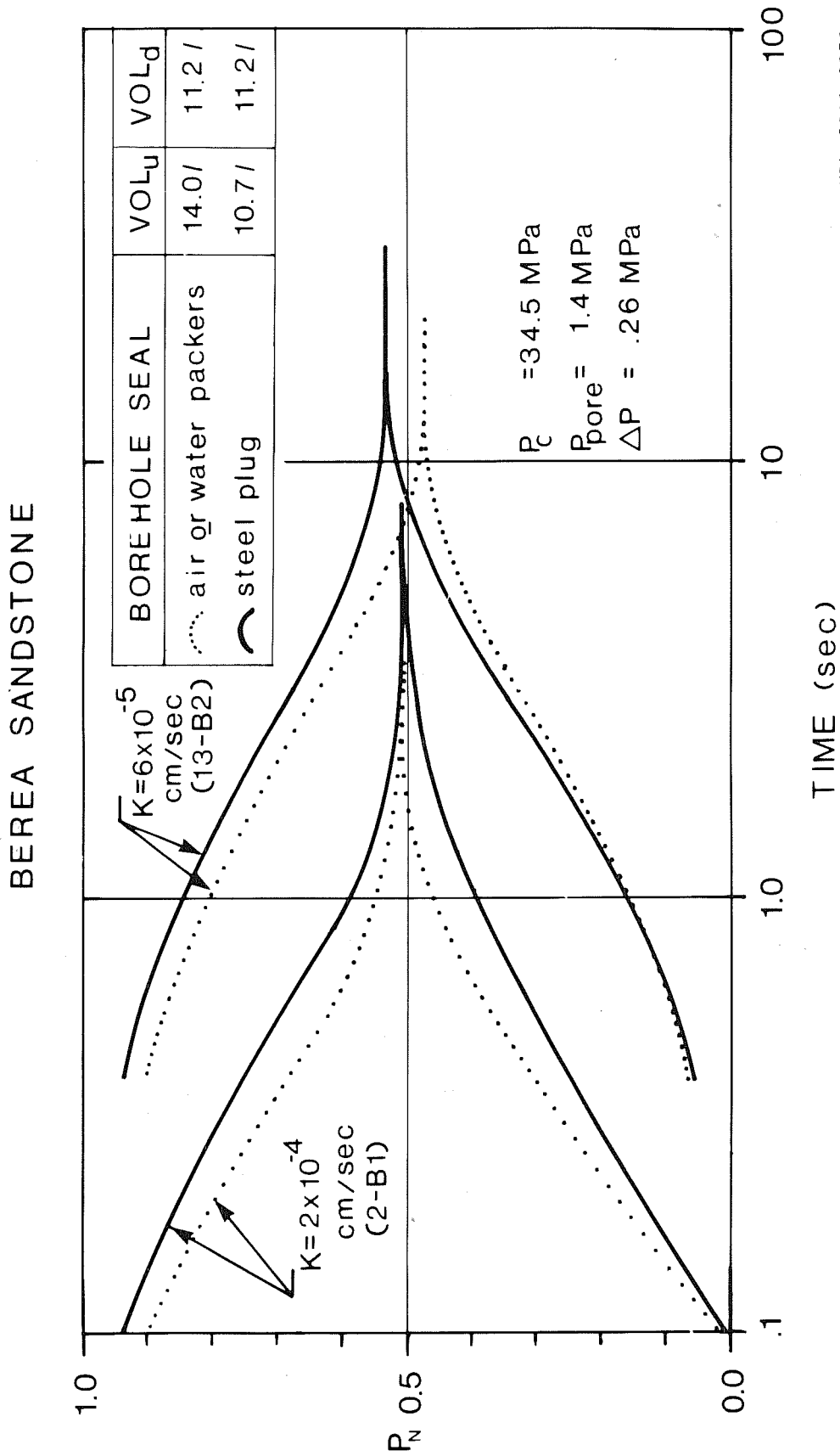
dh = head difference between upstream and downstream sample ends calculated from measured voltage output at upstream and downstream transducers (cm),

k = sample permeability at test temperature (cm²),

K_{pss} = sample conductivity at standard lab temperature of 15.6°C (cm/sec) using porous media assumptions and steady-state test results,

γ_T and μ_T = water properties (weight by density and dynamic viscosity) at measured test temperatures and determined from tables in Weast (1975) (g/ml and cp respectively),

γ_S and μ_S = as above, at standard temperature of 15.6°C ($\gamma_S = 0.999035$ g/ml and $\mu_S = 1.121$ cp).



XBL 8011-3959

Fig. 4.1 Plot of normalized pressure against log time for two sandstone samples.

Calculated conductivity values (Tables 4.1 and 4.2) show that there is a reasonable correlation of the results of K determinations for each sample despite variations in pressure gradients. Sample 2-B1 has a mean average conductivity of 2.4×10^{-4} cm/sec \pm 8% and sample 13-B2 has a mean conductivity of 6.1×10^{-5} cm/sec \pm 11%.

4.1.2 Transient Conductivity Determinations

The results of 15 pressure pulse tests (11 tests of sample 2-B1 and 4 of sample 13-B2) have been reduced and the resulting conductivity values are tabulated in Tables 4.1 and 4.2. With one exception all tests were performed with initial fluid pressures, prior to pulsing (P_{pore}), approximately equal to 1.4 MPa. The same initial fluid and confining pressures were used for each test so as to remove the potential for conductivity variations resulting from variations in these pressures. Various pulse pressures (0.07 to 0.28 MPa) were used in conjunction with the three borehole seals: the water-filled packers, the air-filled packers and the steel plug.

Figure 4.1 shows a plot of normalized pressure P_N against log time. The descending P_N versus log time curves are calculated from the residual upstream reservoir pressure divided by the initial pulse pressure ΔP . The ascending P_N versus log time curves are calculated from the net increase in downstream reservoir pressure divided by the initial pulse pressure. The upstream and downstream reservoirs hold approximately equal volumes of water; thus, the normalized equalization pressure is approximately 0.5. For each sample the general shape of the P_N versus log time curves are similar despite differences in borehole seals. However, tests using the steel plug show a definite increase in decay time, which may be partially attributed

to the effect of the larger upstream reservoir volume used for the steel plug tests. Tests using both water- and air-filled packers provided essentially identical P_N versus log time plots.

Numerical type-curve solutions in the form of P_N versus log time plots have not yet been developed for this test configuration. However, the simplified straight-line technique analysis of Brace et al. (1968) was used to calculate conductivity values from the test results. This technique requires that the a^2 term in the diffusivity equation (Eq. (2.4)) be equal to zero where

$$\frac{\partial^2 P}{\partial x^2} = a^2 \frac{\partial P}{\partial x} \quad \text{and} \quad a^2 = 0, \quad (4.3)$$

thus
$$\frac{\partial^2 P}{\partial x^2} = 0 \quad \text{or} \quad \frac{\partial P}{\partial x} = f(t). \quad (4.4)$$

This implies that the pressure gradient $\frac{\partial P}{\partial x}$ is constant along the sample length and varies with time. Brace et al. likened the test configuration to an electrical circuit where the rock sample acts as a resistor and the two reservoirs act as capacitors. Thus the pressure P_U at any time t in the upstream is given by

$$P_U - P_E = \Delta P [(V_D/V_U) + V_D] e^{-\alpha t}, \quad (4.5)$$

where P_U = upstream pressure, P_E = equalization pressure, ΔP = pressure pulse, V_D = downstream reservoir volume, V_U = upstream reservoir volume, and

$$\alpha = \left(\frac{K}{\mu_T} - \frac{A}{\beta_T L} \right) \left(\frac{1}{V_U} + \frac{1}{V_D} \right) \cdot \frac{\mu_S}{\gamma_S}, \quad (4.6)$$

where β_T = water compressibility at test temperature, μ_T = viscosity of water at test temperature, μ_S = viscosity of water at 15.6°C, and γ_S = weight density of water at 15.6°C.

Equation (4.5) can be restated using normalized pressure P_N where

$$P_N = \frac{P_U - P_E}{\Delta P} = \frac{V_D}{V_U} + V_D e^{-\alpha t} \quad (4.7)$$

Sample conductivity K_{pt} is calculated from the slope (α_{10}) of the plot of normalized and corrected pressure decay P_{NC} against time (Fig. 4.2). Here α_{10} equals α times $\log e$ and P_{NC} is P_N corrected for the difference between upstream and downstream reservoir volumes.

$$P_{NC} = (P_N - C) \frac{1}{1-C} \quad (4.8)$$

where

$$C = \frac{V_U}{V_U + V_D} \quad \left\{ \begin{array}{l} = 0.48 \text{ for steel plug seal} \\ = 0.56 \text{ for packer seal} \end{array} \right.$$

Figure 4.2 shows typical log pressure decay against time plots for both samples. It was noted that for sample 2-B1 the data obtained using both the air-filled packers and water-filled packers yield approximately the same slope ($\alpha_{10} = 0.89$ to 1.10). However the steel plug yields a slightly steeper slope ($\alpha_{10} = 1.10$). This deviation between the slopes of the steel plug data and the water-filled packer data was found (to a lesser degree) for sample 13-B2 (Table 4.2). These deviations are due in part to the difference in the reservoir volumes and in part to the difference in borehole seal compliance. In both cases the water-filled packers appear less compliant than the air-filled packers but more compliant than the steel plug seal.

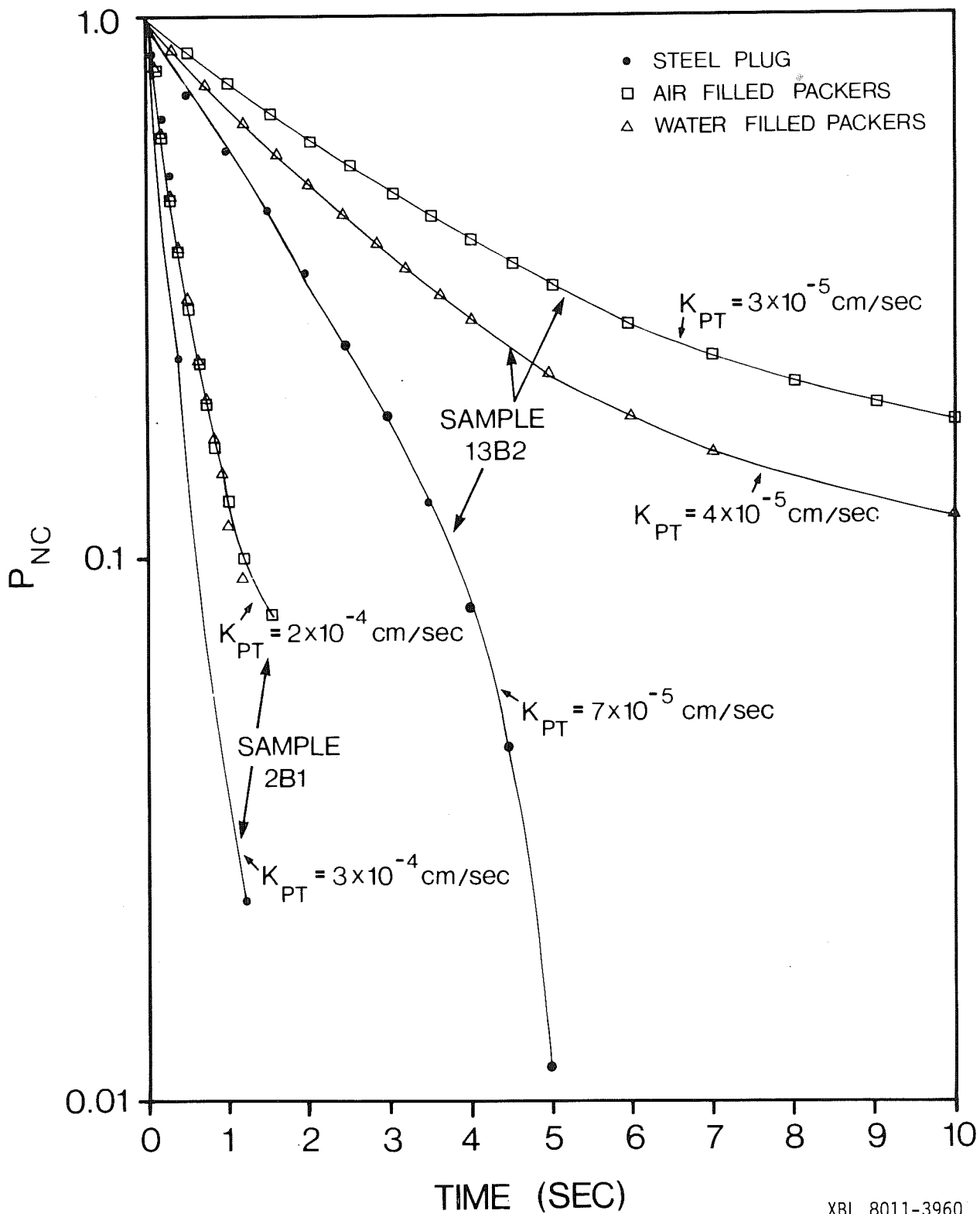


Fig. 4.2 Typical plots of log of corrected normalized pressure decay against time for two sandstone samples.

The straight-line form of the curves indicates that Brace's assumption that $a^2 = 0$ can be used for our high permeability and relatively large sandstone samples. Approximate values of a^2 (Table 4.3) were calculated using data from Zoback and Byerlee (1976). These values are quite small (10^{-7} s/cm² and 10^{-6} s/cm² for samples 2-B1 and 13-B2 respectively), so assuming that $a^2 = 0$ appears reasonable. Thus, it appears that pressures are readily transferred through the sample, providing a gradient that is constant along the sample length and that varies with time. This assumption may not be valid for lower conductivity samples where the pressures are not as readily transmitted through the sample. This follows from Eq. (2.4) where one can see that as permeability k decreases, a^2 increases such that for a conductivity of 10^{-12} cm/sec, a^2 would be approximately equal to 10^3 s/cm², which is certainly much greater than zero.

Conductivity (K) values in Tables 4.1 and 4.2 indicate a reasonable correlation of K values derived from both steady-state (sample 2-B1; 2.4×10^{-4} cm/sec and sample 13-B2; 6.1×10^{-5} cm/sec) and steel plug transient tests (sample 2-B1; 3.1×10^{-4} cm/sec and sample 13-B2; 6.0×10^{-5} cm/sec) performed on each sample. There is also some variation between results of tests performed using the steel plug and tests using standard packers (sample 2-B1 steel plug K , is 130% of air packer K and sample 13-B2 steel plug K is 210% of air packer K). Table 4.1 shows that conductivity values calculated for steel plug (T) tests performed on sample 2-B1 produce slightly higher K values than results of the more compliant packer tests (T_{PW} and T_{PA}). From the conductivity determinations made for sample 13-B1 it appears that varying the type of borehole seal has a similar effect on the resulting K value. Thus, although the plots of P_N versus log time and of log pressure

Table 4.3. Estimate of a^2 for two sandstone samples.

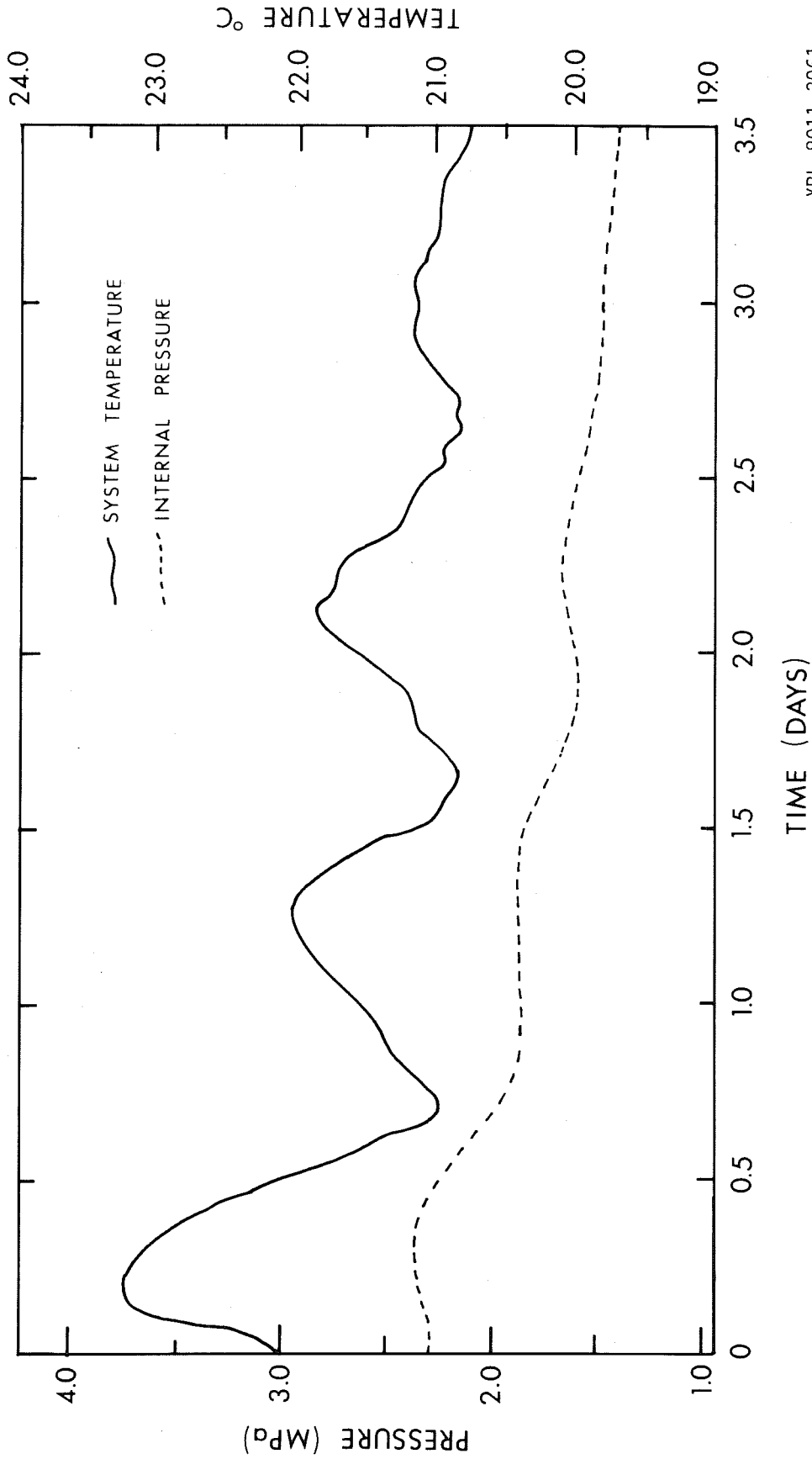
Sample	K_{pss} (cm/sec)	k (cm ²)	n	β_{eff} (Pa ⁻¹)	β_s (Pa ⁻¹)	a^2 (s/cm ²)
13-B2	6.3×10^{-5}	7.3×10^{-8}	~ 0.2	$\sim 8 \times 10^{-11}$	$\sim 3 \times 10^{-11}$	3×10^{-6}
2-B1	2.4×10^{-4}	2.7×10^{-7}	~ 0.2			8×10^{-7}

Note:
$$a^2 = \frac{\mu_t}{k} [-\beta_s(1+n) + \beta_{eff} + \beta_T n]$$

- where
- μ_t = fluid viscosity at the test temperature (P_aS)
 - k = sample permeability from test results (cm²)
 - β_s = compressibility of solid grains (Pa⁻¹)
(from Zoback and Byerlee, 1976)
 - β_{eff} = bulk compressibility of sample) Pa⁻¹)
(from Zoback and Byerlee, 1976)
 - n = sample porosity
 - β_T = compressibility of fluid at test temperature (Pa⁻¹)

versus time show a significant difference in character (dependent upon the borehole seal employed, sample tested, and reservoir volumes), the resulting K values for each sample are similar (sample 2-B1 transient K is 130% of steady-state K and sample 13-B2 transient K is also 130% of steady-state K).

During the test program it was noted that variations in room temperature caused pressure variations within the system due to the effects of thermal expansion of water. Reservoir pressure and temperatures were monitored over a 3.5-day period to determine the magnitude of the pressure variations (Fig. 4.3) for comparison with a theoretical determination. From Fig. 4.3, a pressure decrease of approximately 1 MPa corresponds to a temperature decrease of approximately 2.5°C. If only the thermal expansivity of water is considered (data from Weast, 1975) the fluid volume is increased by 10 cc and the fluid pressure decreased by 1.4 MPa for a drop of 2.5°C (calculations discussed in Chapter 3 indicate that negligible volume changes result from thermal or pressure deformation of the reservoirs). A pressure increase in the upstream reservoir of 0.33 MPa which results from a displacement of 10 cc within the complete system should cause a pressure change of approximately 0.8 MPa. The elasticity of the packers is assumed to reduce the theoretical pressure change of 1.4 MPa/2.5°C to the observed value in the order of 0.8 MPa/2.5°C or less. In order to monitor the temperature variations that could produce a pressure change of 0.007 MPa (10% of the lowest pulse pressure used in this experiment), temperature variations of less than 0.03°C must be identifiable. To reduce the overall variation in temperature a thermal bath was constructed to keep the complete test configuration at room temperature with minimal variation (less than 0.03°C). In order to monitor these small temperature differences, thermistors with an accurate resolution



XBL 8011-3961

Fig. 4.3 Correlation of pressure and temperature variations.

of 0.01°C were also installed in the system.

Strains in the order of 5 to 10 microstrain ($\mu\epsilon$) were measured (in response to a 0.3 MPa pressure pulse) by a circumferential strain gauge attached to the borehole. The Budd strain readout box is reported to have an accuracy of approximately 5 $\mu\epsilon$; thus the strain readings obtained are not of high quality. However, measured strains are similar in magnitude to strains calculated from the elastic properties of the steel pipe (Chapter 3). Thus it appears that the deformation of the simulated borehole during the laboratory pressure pulse tests will cause minimal volume change effects. Strains have not been measured in the bar which connects the two packers (due to equipment difficulties), thus the magnitude of packer separation in the borehole has not been verified.

4.2 Stripa Granite Sample With a Single Fracture - Test Results

4.2.1 Steady-State Conductivity Determinations

The results of steady state conductivity tests performed on the granite sample have been used to calculate various effective fracture apertures ($2b_{eff}$) and fracture conductivities (Table 4.4). Test procedures were similar to those described in Chapter 3 and Appendix II. However, due to the low sample permeability it was considered necessary to minimize and monitor temperature variations during both steady-state and transient tests. Thus the equipment was submerged in a trough containing approximately 3600 liters of water. In addition, thermistors with a sensitivity of 0.01°C were used to monitor temperature variations during testing. The capability of maintaining elevated pore pressures during flow tests was added to the system in order to provide the best correlation between steady-state and transient tests per-

Table 4.4. Steady state flow tests, Stripa granite with a single fracture.

Loading Cycle	Confining Pressure P_C (MPa)	Flow Q (cm^3/sec) $\times 10^2$	Q/h (cm^2/sec) $\times 10^6$	$2b_{\text{eff}}$ (cm) $\times 10^3$	K_{fss}^* (cm/sec) $\times 10^2$	K_{pss}^* (cm/sec) $\times 10^6$
1	3.4	2.6	11.8	1.4	1.41	4.6
1	6.9	0.89	4.06	0.98	0.69	1.6
1	10.3	0.40	1.57	0.71	0.36	0.61
1	13.8	0.22	1.02	0.62	0.28	0.40
3	3.4	0.84	3.89	0.97	0.67	1.52
3	6.9	0.38	1.76	0.74	0.39	0.69
3	10.3	0.23	1.07	0.63	0.29	0.42
3	13.8	0.17	0.79	0.57	0.23	0.31
4	3.4	1.35	18.8	1.63	1.9	7.36
4	3.4	1.24	13.3	1.46	1.59	5.21
4	3.4	1.60	10.7	1.35	1.31	4.19
4	3.4	2.32	14.7	1.51	1.63	5.75
4	3.4	2.15	13.7	1.47	1.55	5.36
4	3.4	2.53	16.4	1.56	1.74	6.42
4	6.9	0.81	5.19	1.06	0.81	2.03
4	6.9	0.51	3.27	0.91	0.59	1.28
4	6.9	0.51	3.27	0.91	0.59	1.28
4	6.9	0.53	3.33	0.92	0.61	1.30
4	6.9	0.49	3.74	0.95	0.65	1.46
4	13.8	0.13	1.01	0.62	0.28	0.40
4	13.8	0.12	0.95	0.60	0.26	0.37
4	13.8	0.08	0.60	0.52	0.19	0.23
4	13.8	0.09	0.67	0.54	0.21	0.26
4	13.8	0.08	0.65	0.53	0.20	0.25

*Conductivity calculated at 15°C.

formed on the fractured granite. If the pore pressures applied during steady-state tests differ from those applied during transient tests, then changes in fracture aperture between each test due to different effective stresses would cause conductivity differences. Thus, the equipment was modified from the configuration of Fig. 3.1 by attaching a nitrogen bottle and regulator to the downstream reservoir outlet and adjusting the downstream pressure to the equivalent of an in-situ pore pressure.

Flow rates were measured at confining pressures of 3.6, 6.9, 10.3 and 13.8 MPa during the ascending portions of various loading cycles. A single loading cycle consists of: i) a stepwise increase in confining pressure from 0.0 MPa to the maximum of 13.8 MPa and ii) a stepwise decrease in confining pressure from 13.8 MPa to 0.0 MPa. A constant pressure difference of 0.14 MPa was applied across the sample with pore pressure of 1.38 MPa throughout the system. Figure 4.4 is a plot of confining pressure (P_C) against flow rate (Q) over head difference (h) or Q/h which shows the exponential decrease in flow rate with increasing confining pressure. Cycle #1 yielded the greatest flow rates at each confining pressure, while Cycle #3 yielded the lowest, except at $P_C=13.8$ MPa, where Cycle #4 yielded a minimum flow rate. Only a few transient tests were performed during Cycle #1 and none during Cycle #3. Thus it appears that transient and steady-state tests performed during Cycle #4 tend to cause variations in the fracture permeability, perhaps by washing of particles from the fracture or propping of the fracture. Minimal temperature variations were observed during testing; thus temperature influences are not expected to have contributed to the flow rate variations observed in Cycle #4.

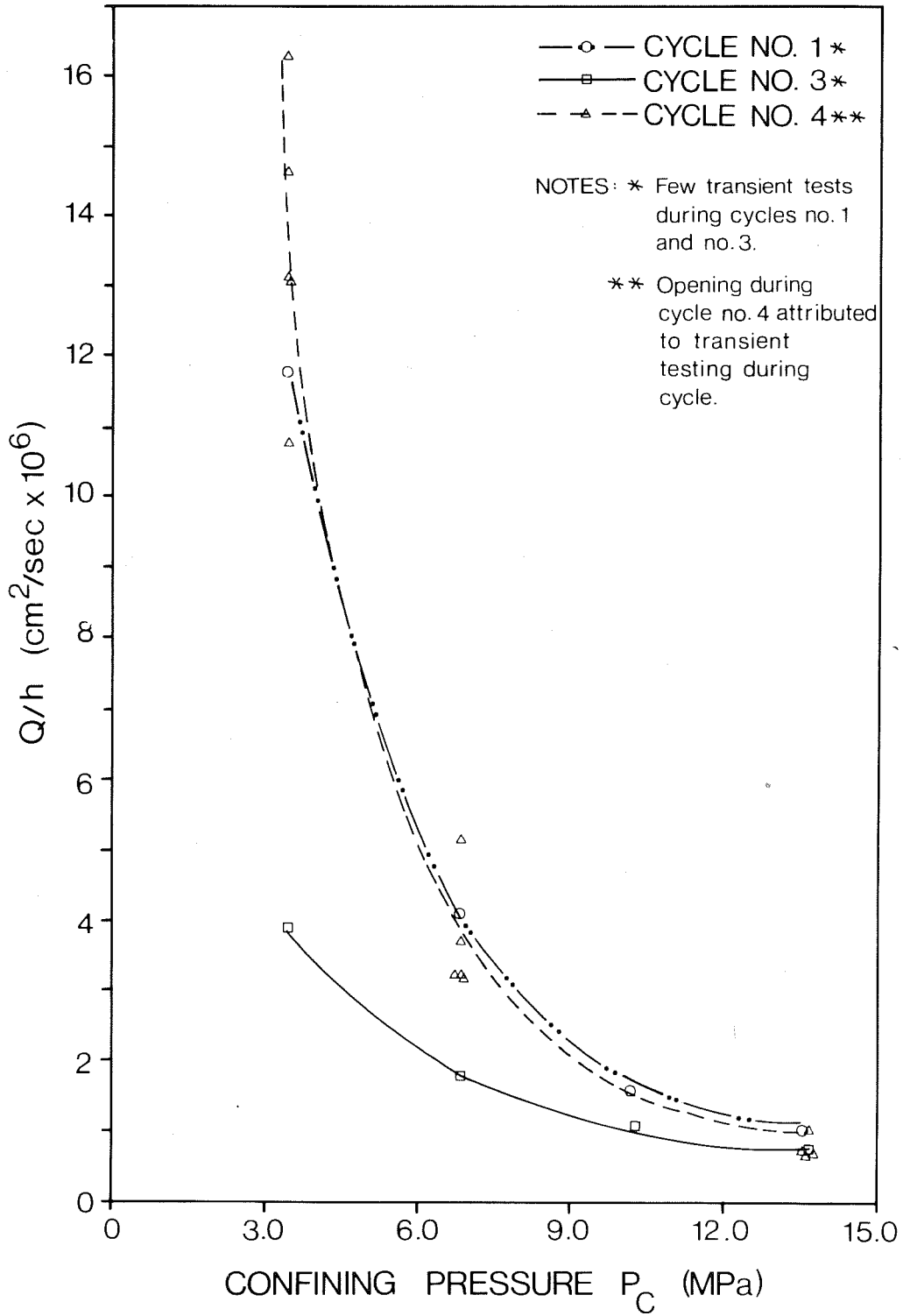


Fig. 4.4 Confining pressure against flow rate - Stripa granite.

Steady-state fracture conductivities (K_{fSS}) were calculated from flow test data assuming the parallel plate flow law and Eq. (4.2). Thus

$$K_{fSS} = \frac{k_f V_s}{\mu_s} = -q \frac{\gamma_s}{\gamma_T} \cdot \frac{dv}{dh} \cdot \frac{1}{A} \cdot \frac{\mu_T}{\mu_s} \quad (4.9)$$

or

$$k_f = \frac{2b^2 \gamma_s}{12 \mu_s} = -q \cdot \frac{\gamma_s}{\gamma_T} \cdot \frac{dx}{dh} \cdot \frac{1}{A} \cdot \frac{\mu_T}{\mu_s} \quad (4.10)$$

Initially effective fracture apertures ($2b_{eff}$) were calculated as the cross section area of flow -- $2b$ times the core diameter W .

Thus

$$2b_{eff} = \sqrt[3]{\frac{q \cdot 12 \cdot \mu_T \cdot dx}{W \cdot dh \cdot \gamma_T}} \quad (4.11)$$

and

$$k_f = \frac{(2b_{eff})^2 \cdot \gamma_s}{12 \mu_s} \cdot \quad (4.12)$$

A summary of fracture conductivity (K_{fSS}) at different confining pressures as calculated from measured flow rates during Cycle #4 is as follows

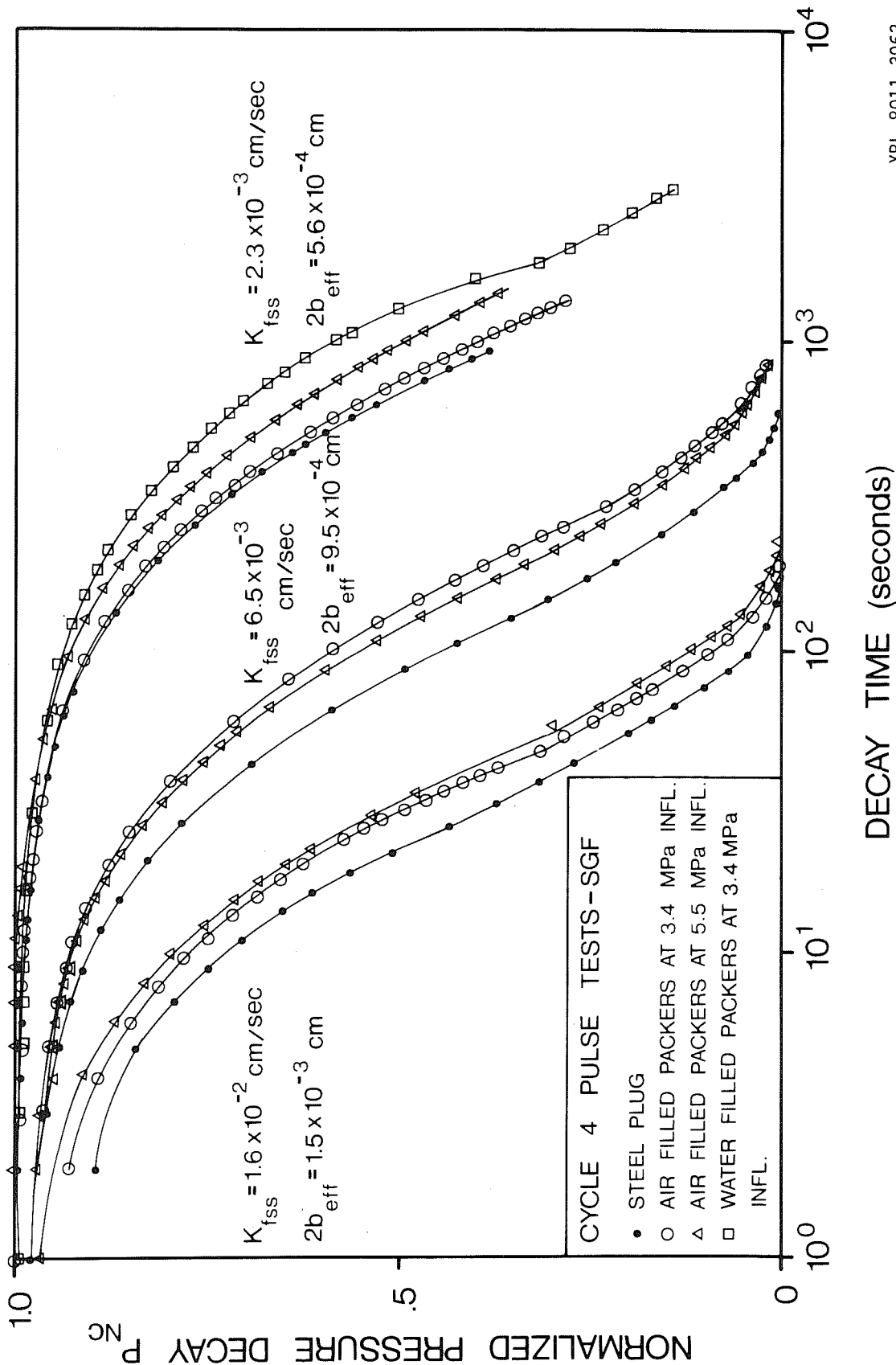
Confining pressure (MPa)	$K_{fSS} \times 10^2$ cm/sec
3.4	1.6 ± 9%
6.9	0.65 ± 20%
13.8	0.23 ± 20%

This indicates variations of up to ±20% in steady-state conductivity values caused by both transient and steady-state tests during the cycle.

4.2.2 Transient Conductivity Determinations

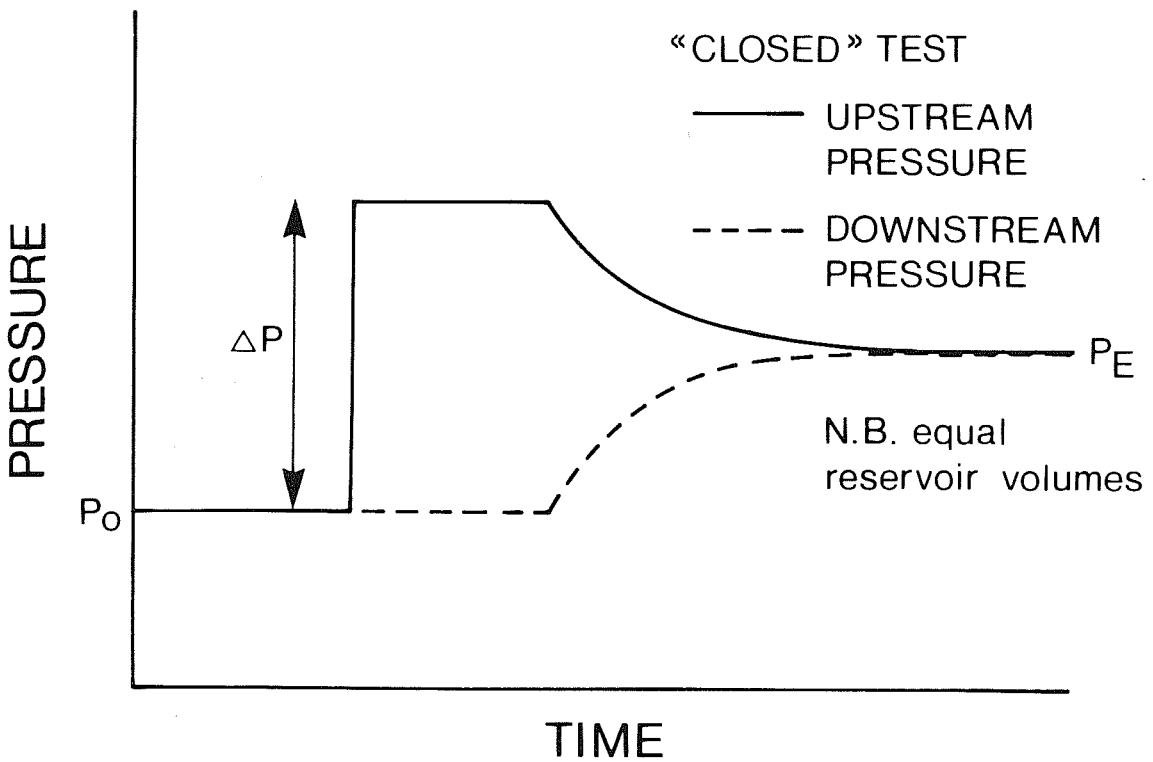
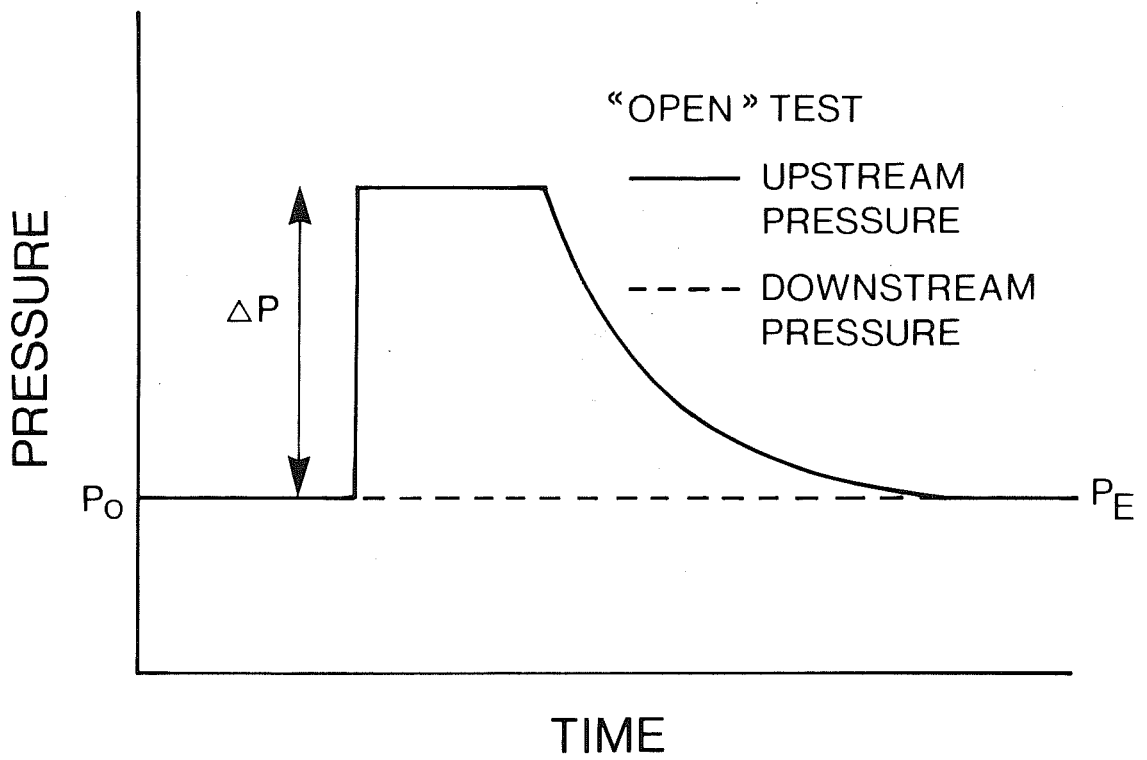
The results of transient pressure pulse conductivity tests performed on the granite sample during loading (Cycle #4) have been plotted and a summary plot is presented in Fig. 4.5. Test procedures were similar to those described in Chapter 3 and Appendix II. In addition to the modifications of equipment and procedures described in the previous section, further modifications were required to perform pressure transient tests on the granite. In section 4.1 it was noted that the upstream reservoir volume in the steel plug configuration differed from the reservoir volume in the double packer configuration. Thus steel rods were inserted into the full length borehole (when sealed with the steel plug) to make the upstream reservoir volume in both cases equal to 11.2 l. This provides a much better opportunity for correlation between the results obtained from tests performed with different borehole seals. Using the modifications designed to regulate the downstream reservoir pressure (previous section), transient tests were performed with a constant pressure downstream boundary (equivalent to an infinite downstream reservoir volume) condition rather than a zero flow boundary condition. Tests performed on sandstone samples were all of the zero flow or "closed" type (Fig. 4.6) while transient tests of the granite were of both the constant downstream pressure or "open" type (Fig. 4.6) and the "closed." In comparing the results of different transient tests on the granite sample, it was found more convenient to consider the "open" type test results rather than the "closed" results discussed in section 4.1.

The normalized pressure versus log time plot of Fig. 4.5 shows the results of transient tests performed at three confining pressures (3.4, 6.9 and 13.8 MPa) in conjunction with the flow tests described in the pre-



XBL 8011-3963

Fig. 4.5 Stripa granite with single fracture - loading cycle #4.



XBL 8011-3964

Fig. 4.6 Schematic comparison of pressure versus time plots for "open" and "closed" boundary conditions.

vious section. All tests were performed at a pore pressure of 1.4 MPa with pulse pressures of 0.07 and 0.14 MPa. Similar to the results of section 4.1, it was found that the test results were independent of the magnitude of the pressure pulse. Thus, the results shown in Fig. 4.5 reflect test results using both 0.07 and 0.14 MPa pressure pulses.

The borehole seals used were: i) steel plug, ii) air-inflated packers at 3.4 MPa, iii) air-inflated packers at 5.5 MPa and iv) water-inflated packers at 3.4 MPa. The plot of Fig. 4.5 indicates that in all cases the steel plug configuration provides the shortest decay time. The different packer configurations provide different decay times but similar curve shapes for each group of tests. The water-filled packers provided the longest test time. There is no definite trend in the effects of variation of the packer inflation pressure. This lack of resolution may be partially attributable to the variation in conductivities calculated from flow rates measured between each test series. Also, the water-filled packers caused greater difficulties in minimizing pressure variations caused by leakage and temperature effects. Because of the low compressibility of water, a small leak of water from the packer can cause considerable pressure variations in the test cavity. In addition, variations in water temperature in the packers can cause significant pressure changes due to the thermal expansivity of water. Type curves are not yet available for analysis and calculation of fracture conductivities from Fig. 4.5.

The results of 23 pulse tests (6 closed and 18 open tests) performed on the granite sample have been reduced and conductivities calculated using Brace's straight-line technique (Table 4.5). Figure 4.7 shows the typical

Table 4.5. Transient test results of Cycle #4.

Test No.	Seal	P_C (MPa)	ΔP (MPa)	α_{10} (sec^{-1}) $\times 10^2$	$2b_{\text{eff}}$ (cm) $\times 10^4$	K_{ft} (cm/sec) $\times 10^3$	K_{pt} (cm/sec) $\times 10^7$
SPI2505	✓	3.4	0.04	1.90	13.4	12.9	88
SPI10050	✓	3.4	0.02	1.59	16.3	19.0	71
SPI20050	✓	3.4	0.14	1.41	15.6	17.4	64
AP5I10050	✓	3.4	0.07	1.27	15.1	16.3	58
AP5I20050	✓	3.4	0.14	1.11	14.4	14.9	51
AP8I20050	✓	3.4	0.14	1.02	14.0	14.1	46
AP8I2005C	✓	3.4	0.14	2.27	18.3	24.0	51
SPI10400	✓	6.9	0.07	0.357	9.89	7.01	16
SPI20100	✓	6.9	0.14	0.364	9.50	7.10	17
AP5I10100	✓	6.9	0.07	0.242	8.69	5.41	11
AP5I20100	✓	6.9	0.14	0.227	8.50	5.18	10
AP8I20100	✓	6.9	0.14	0.251	8.79	5.54	11
SPI10200	✓	13.8	0.07	0.046	5.00	1.79	2.1
SPI1020C	✓	13.8	0.07	0.094	6.34	2.88	2.1
SPI20200	✓	13.8	0.14	0.052	5.21	1.95	2.3
SPI2020C	✓	13.8	0.14	0.092	6.30	2.85	2.1
AP5I10200	✓	13.8	0.07	0.041	4.81	1.66	1.9
AP5I1020C	✓	13.8	0.07	-----	non-linear	-----	-----
AP5I20200	✓	13.8	0.14	0.042	4.84	1.68	1.9
AP5I2020C	✓	13.8	0.14	-----	non-linear	-----	-----
AP8I20200	✓	13.8	0.14	0.033	4.45	1.42	1.5
AP8I2020C	✓	13.8	0.14	0.063	5.56	2.22	1.5
WP5I20200	✓	13.8	0.14	0.023	3.98	1.14	1.1

Steel Plug
Air Packers
Water Packers

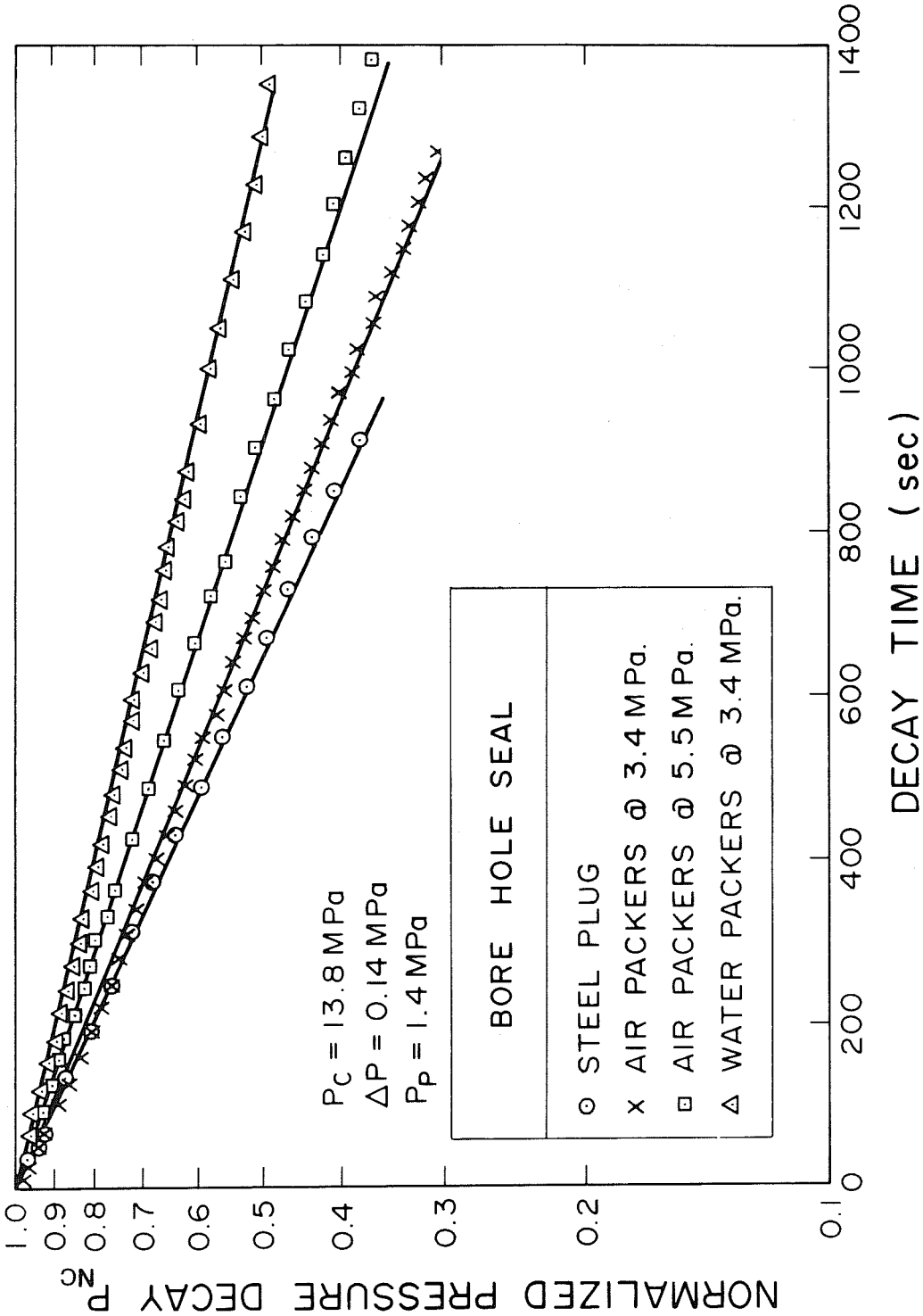


Fig. 4.7 Typical plot of log of normalized pressure decay against time for a granite sample containing a single fracture.

log-linear plot of normalized corrected pressure P_{NC} against time for the granite sample at a confining pressure P_C of 13.8 MPa. The straight-line nature of the plot suggests that $a^2 \cong 0$ (as discussed in section 4.1.2). A value of $a^2 = 3 \times 10^{-5}$ sec/cm² was estimated at a confining pressure of 13.8 MPa using the calculations outlined in Table 4.3 and data from Brace et al. (1968). This value is sufficiently small that the assumption of $a^2 \cong 0$ appears reasonable. Values of conductivity were calculated for the sample using Brace's technique modified for a parallel plate rather than porous-media flow (as outlined by Kranz et al., 1979) and are shown in Table 4.5. A summary of conductivity results is shown in Table 4.6 for comparison. This table shows that open tests tend to give slightly lower calculated conductivities than closed tests. In addition it can be seen that packer compliance becomes increasingly important with increasing confining pressure or decreasing sample conductivity. At the lowest confining pressure ($P_C = 3.4$ MPa), steel plug results supersede packer results by a maximum of 50%. However, at the highest confining pressure ($P_C = 13.8$ MPa), steel plug results supersede packer results by a maximum of 100%. The correlation between steady-state and transient test results is good overall; however, there appears to be a tendency for poorer correlation with decreasing sample conductivity.

Table 4.6. Comparison of steady-state and transient test results (granite sample - Cycle #4).

P _c (MPa)	Borehole seal	Mean K _f (cm/sec)x10 ³		Mean K _p (cm/sec)x 10 ⁷		
		Steady state	Transient Open Closed	Steady state	Transient Open Closed	
3.4	Steel plug		16	--	74	--
	Air packers @ 3.4 MPa		16	--	54	--
		16			56	
	Air packers @ 5.5 MPa		14	24	46	51
	Water packers @ 3.4 MPa		--	--	--	--
6.9	Steel plug		7	1	17	--
	Air packers @ 3.4 MPa	6.5	5.4	--	15	11
	Air packers @ 5.5 MPa		5.5	--	11	--
	Water packers @ 3.4 MPa		--	--	--	--
13.8	Steel plug		1.9	2.9	2.2	2.1
	Air packers @ 3.4 MPa	2.2	1.7	--	2.9	1.9
	Air packers @ 5.5 MPa		1.4	2.2	1.5	1.5
	Water packers @ 5.5 MPa		1.1	--	1.1	--

5. SUMMARY AND CONCLUSIONS

Previous workers have proposed the pressure pulse test technique as an alternative to standard conductivity tests performed, on low-permeability fractured or unfractured rock. However, the pressure pulse test has not been calibrated against steady-state conductivity measurements, nor have attempts been made to calibrate or assess the contribution of the test equipment response to the pressure-time curve.

The theory of pressure pulse tests as described by Brace et al. (1968), Lin (1977) and Wang et al. (1977) has been reviewed. Discussion has focussed on the test conditions inherent in the basic theory, and modifications have been proposed that should allow one to develop type curves for the analysis of laboratory tests on deformable fracture samples. These modifications incorporate a stiffness coefficient that simulates part of the response, or compliance, of the packer assembly due to the applied pressure pulse.

This report describes the equipment and procedures used to investigate the correlation of permeability values from transient and steady-state laboratory tests on rock samples. The experimental apparatus was specifically designed to investigate the effects of the compliance of standard field packers (in a full-scale simulated borehole) on transient test results.

Both steady-state and transient conductivity tests were carried out on two samples of Berea sandstone and one sample of the Stripa granite. The granite sample contained a natural fracture parallel to the core axis. A summary of test results for the sandstone samples is presented in Table 5.1 and for the granite sample in Table 5.2.

Table 5.1. Comparison of average steady-state and transient K determinations for sandstone samples.

Sample No.	Steady-state K_{pss} (1) (cm/sec)	Transient K_{pt} (2) (cm/sec)	Borehole seal	% Ratio (2)/(1)
2-B1	2.4×10^{-4}	2.6×10^{-4}	All	108%
		2.3×10^{-4}	Air packers @ 3.4 MPa	96%
		2.7×10^{-4}	Water packers @ 3.4 MPa	113%
		3.1×10^{-4}	Steel plug	130%
13-B2	6.1×10^{-5}	4.0×10^{-5}	All	65%
		2.5×10^{-5}	Air packers @ 3.4 MPa	41%
		3.5×10^{-5}	Water packers @ 3.4 MPa	57%
		6.0×10^{-5}	Steel plug	98%

Table 5.2. Comparison of average steady-state and open-test transient K determinations for the granite sample.

Pc (MPa)	Steady-state K_{fss} (cm/sec) x 10^3	Transient K_{ft} (cm/sec) x 10^3	Borehole seal
3.4	16	16	All
		16	Air packers @ 3.4 MPa
		14	Air packers @ 5.5 Mpa
		16	Steel plug
6.9	6.5		All
		5.4	Air packers @ 3.4 MPa
		5.5	Air packers @ 5.5 MPa
		7.1	Steel plug
13.8	2.2		All
		1.7	Air packers @ 3.4 MPa
		1.4	Air packers @ 5.5 MPa
		1.1	Water packers
		1.9	Steel plug

The transient tests on the sandstone and granite samples were analyzed using the simplified technique of Brace et al., which assumes that the pressure gradient is constant along the sample length ($a^2 = 0$ in Eq. (4.2)) and hence varies only as a function of time. This appears to be a reasonable assumption for these relatively high permeability samples, as a^2 is in the order of 10^{-6} or 10^{-7} sec/cm² for the two sandstone samples and in the order of 10^{-5} sec/cm² for the granite sample.

From Table 5.1 it can be seen that transient tests on the porous media samples produced conductivity values that ranged from 57% to 130% of the equivalent steady-state test. This deviation is assumed to result, in part, from the effects of packer compliance; however, in the initial series of tests, the full significance of packer compliance is obscured because:

- i) Short test times (4 to 20 sec) are at the sensitivity level of the recording equipment. Thus it is difficult to obtain results with a high level of accuracy.
- ii) Temperature variations greater than 0.03°C were measured and these have been shown by experiment, and by using basic physical principles, to cause variations in fluid pressures that could easily mask the effects of packer compliance. Pressure or fluid leaks during testing can also have such an effect on test results. Pressure variations caused by temperature fluctuations and pressure leaks may not be of great significance in the short (4-20 sec) tests of the sandstone samples, but for tests of lower permeability samples, with decay times of minutes to hours, control of these factors is critical.

iii) Major assumptions made in developing the theory for analyzing the test results may not be completely satisfied. These assumptions would include: (1) homogeneous and isotropic samples, (2) instantaneous pulse application, (3) constant gradient along the sample, and (4) a^2 in Eq. (4.2) is approximately equal to 0. The sandstone samples were cored parallel to the observed anisotropy in an attempt to fit these assumptions as closely as possible. However, any significant deviation could cause the observed differences between the steady-state and transient conductivity determinations. Also, a pulse application time of 1 to 2 seconds, when compared to the 6-second decay time of sample 2-B1, is certainly not instantaneous. This is shown in Fig. 5.1a, where the effects of closed or laboratory-type test conditions are compared with the effects of open or field-type test conditions. Calculated values of a^2 are in the order of 10^{-6} to 10^{-7} sec/cm²; thus a^2 can be reasonably assumed to be equal to zero.

From Table 5.2 it can be seen that transient tests of the granite sample produced conductivity values ranging from 50% to 110% of the equivalent steady-state test. This deviation is presumed to result dominantly from the effects of packer compliance. The lower-permeability granite yields much longer test times, which enables accurate measurements with the recording system used. Temperatures were monitored throughout each test and found to vary well within the $\pm 0.01^\circ\text{C}$ range required to minimize temperature effects. The time of pulse application (1 to 2 seconds) was essentially instantaneous when compared to decay times in the order of minutes or hours. Since the value of a^2 in Eq. (4.2) was found to be approximately 10^{-5} , reasonably

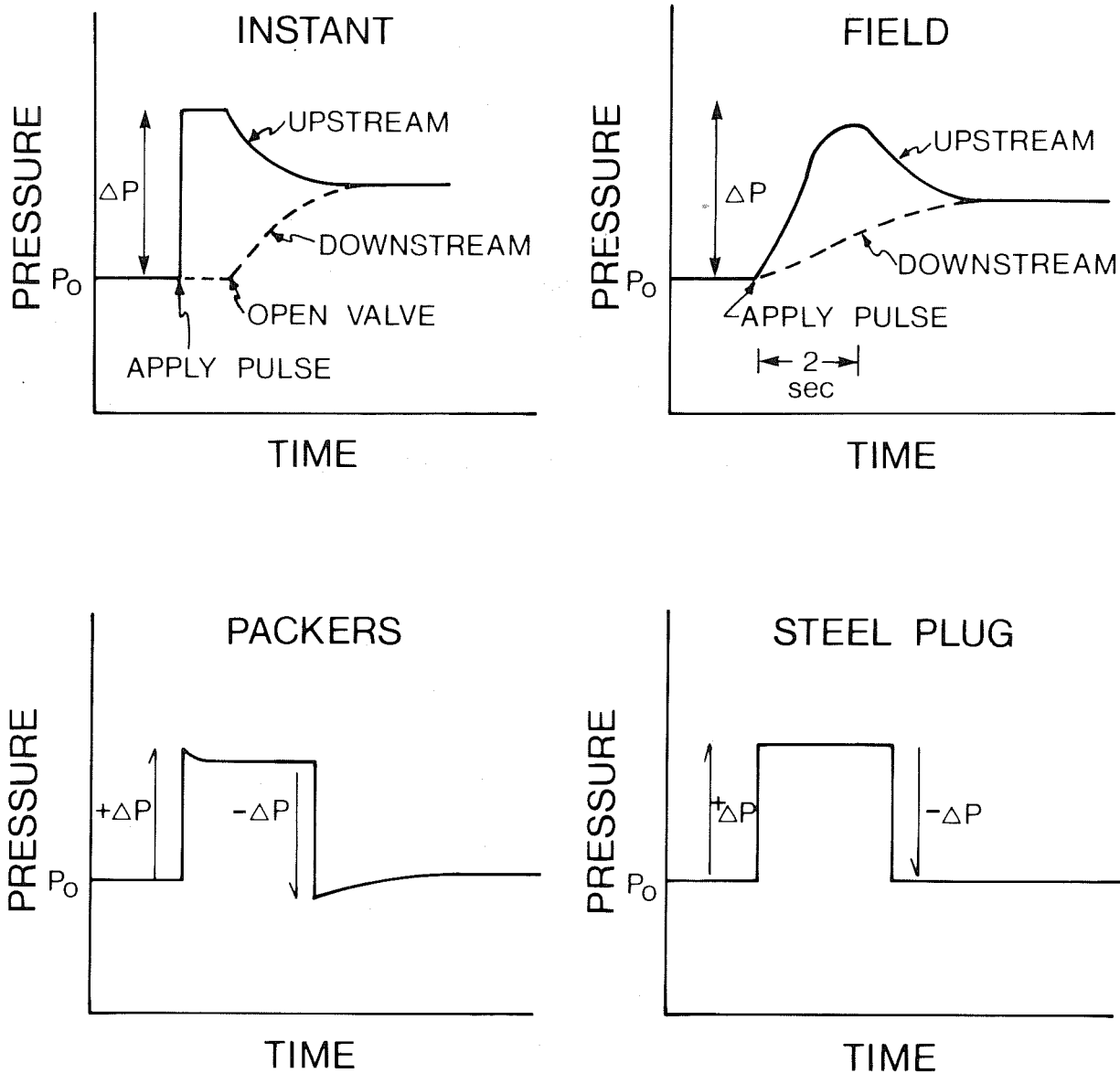
close to zero, the use of Brace's technique for conductivity calculation was validated. Although the comparative results are unfortunately somewhat obscured by fracture conductivity changes caused by steady-state and transient testing of the sample, reproducible results were obtained.

In testing of the sandstone samples water-inflated packers tended to show less compliance than air-inflated packers. However, for the granite sample the water inflated packers showed more compliance than air-inflated packers. This discrepancy is a direct result of the larger pressure responses produced by small variations in packer volume when filled with water rather than air. It appears that the longer test times at lower conductivities amplify this problem, particularly when considering packer volume variations due to external temperature and/or pressure variation.

Thus, any borehole test assembly should be thoroughly checked in a full-scale laboratory assembly, such as is described in this report, before being used to carry out field tests. This check will permit one to identify the assembly response and hence separate it from the pressure-time curve obtained from testing a given section of the borehole.

The creep effects shown in Fig. 5.1 suggest that stiff packers should be selected for use in pressure-pulse packer assemblies. In addition, in order to be able to interpret field results, pressure pulse packer assemblies must incorporate devices capable of measuring temperature variations of $\pm 0.01^\circ\text{C}$ in the isolated cavity.

In the high-conductivity sandstone samples, transient tests tend to give lower estimates of permeability. As permeability decreases (as in the



XBL 8011-3966

Fig. 5.1 Effect of boundary conditions on system response.

granite sample) and the compliance effects become greater; hence, if no corrections are made, the difference between steady-state and transient test results becomes greater. This deviation between steady-state and transient tests may result in part from the variation in sample conductivity. However, with decreasing conductivity, the values of a^2 increase such that at a sample conductivity of 10^{-12} cm/sec, $a^2 = 10^3$ sec/cm. Thus in very low conductivity ranges Brace's technique may no longer be valid for calculating transient conductivity values and a more sophisticated numerical analysis is required.

6. ACKNOWLEDGMENTS

This study was supported by funds from the Lawrence Berkeley Laboratory, provided through the Waterloo Research Institute under contract WRI 708-04, and from the National Research Council of Canada through an operating research grant to J.E. Gale. This study has benefited from active discussions with P.A. Witherspoon and J. Wang of LBL and W. Brace of MIT.

7. REFERENCES

- Bouwer, H. and R.C. Rice, 1976. A slug test for determining hydraulic conductivity of unconfined aquifers with completely or partially penetrating wells, Water Resources Research, Vol. 12, No. 3, pp. 423-428.
- Brace, W.F., J.B. Walsh, and W.T. Frangos, 1968. Permeability of granite under high pressure, J. Geophys. Res., Vol. 73, No. 6, pp. 2225-2236.
- Bridgman, P.W., 1958. The physics of high pressure. G. Bell and Sons, London.
- Clarke, J.P. Jr., 1966. Handbook for physical constants, Geol. Soc. Amer., Mem. 97.
- Cooper, H.H., J.D. Bredehoeft, and I.S. Papadopoulos, 1967. Response of finite-diameter well to an instantaneous charge of water, Water Resources Research, Vol. 7, No. 1, pp. 263-269.
- Earlougher, R.C., 1977. Advances in well test analysis, Society of Petroleum Engineers of AIME, Mono. No. 5.
- Gale, J.E., and P.A. Witherspoon, 1979. An approach to the fracture hydrology at Stripa - Preliminary Results: Sem. on In-Situ Heating Experiments in Geologic Formations; Org. Econ. Coop. Dev. Ludvika, Sweden, Lawrence Berkeley Laboratory report LBL-7079 (SAC-15).
- Gale, J.E., 1980. Assessing the permeability characteristics of fractured rock, Proceedings of Recent Trends in Hydrogeology Symposium. GSA Special Publication. In press.
- Hodgen, A., E.H. Ohlsen, W. Stiles, and J.A. Weast, 1967. Mechanics of materials, John Wiley and Sons, Inc.
- Hvorslev, M.J., 1951. Time lag and soil permeability in groundwater observations. U.S. Army Waterways Expt. Station, Vicksburg, Mississippi (Bull. No. 36).
- Kranz, R.L., A.D. Frankel, T. Engleleider, and C.H. Schloz, 1979. The permeability of whole and jointed Barre granite, Int. J. Rock Mech. Min. Sci. and Geomech. Absts., Vol. 16. pp. 225 to 234.
- Olkiewicz, A., J.E. Gale, R. Thorpe, and B. Paulsson, 1979. Geology and Fracture System at Stripa. Lawrence Berkeley Laboratory report LBL-8907, (SAC-21).
- Lin, W., 1977. Compressible fluid flow through rocks of variable permeability, Lawrence Livermore Laboratory, University of California.
- Papadopoulos, I.S., J.D. Bredehoeft, and H.H. Cooper, 1973. On the analysis of slug test data, Water Resources Research, Vol. 9, No. 4, pp. 1087-1089.

- Swan, G., 1978. The Mechanical properties of Stripa granite. Lawrence Berkeley Laboratory report LBL-7074 (SAC-03).
- Walsh, J.B., 1965. The effect of cracks on the compressibility of rock. J. Geophys. Res., Vol. 70, pg. 381.
- Wang, J.S.Y., T.N. Narasimhan, C.F. Tsang, and P.A. Witherspoon, 1977. Transient flow in tight fractures, Proceedings of Invitational Well-Testing Symposium, October, 1977, Berkeley, California.
- Weast, R.C., 1975. Handbook of chemistry and physics, CRC Press, Cleveland, Ohio.
- Zoback, M.D. and J.D. Byerlee, 1976, A note on the deformation fluid flow behavior of crushed granite, Int. J. Rock Mech. Min. Sci., Vol 13, p. 291.

APPENDIX I

DEVELOPMENT OF EQUATIONS TO DESCRIBE PRESSURE PULSE TESTS PERFORMED ON A CYLINDRICAL SAMPLE UNDER HYDROSTATIC COMPRESSION

Using the basic principles outlined in Chapter 2, the governing equations for pulse testing of porous samples will be determined following the work of Brace et al. (1968) and Lin (1977). Some modifications will be made to the equations developed by Brace et al. and Lin in order to derive the equations governing tests performed on samples containing a single fracture and to simulate the effects of packer compliance.

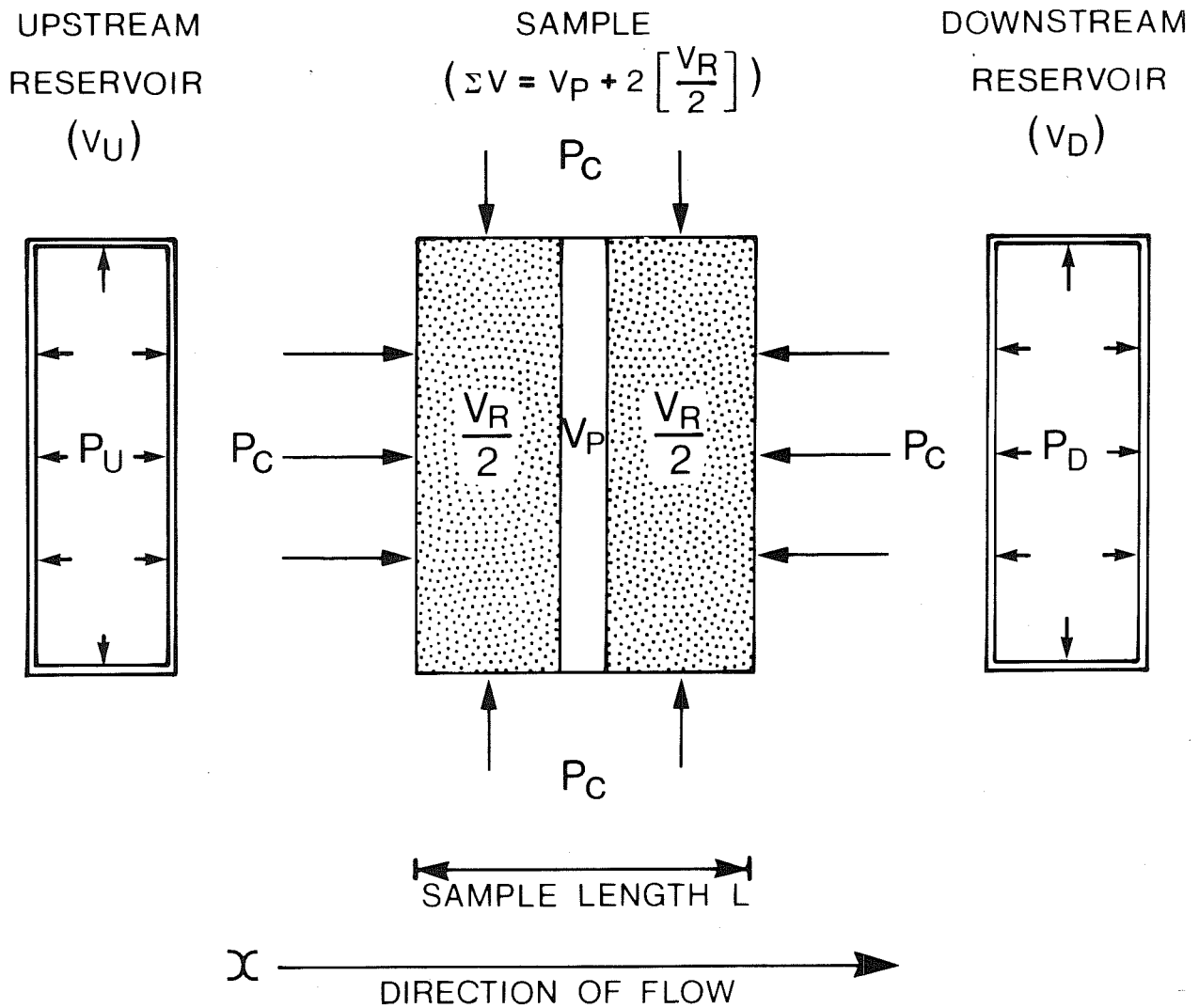
I.1 Porous Cylindrical Sample

A schematic of the porous cylindrical rock sample subjected to hydrostatic compression is shown in Fig. I.1. The rate of fluid flow through the rock sample under an imposed gradient $\frac{dp}{dx}$ is a function of fluid viscosity μ , rock permeability k , and cross-sectional area A .

Differentiating Darcy's law ($q = \frac{-Ak}{\mu} \cdot \frac{dp}{dx}$) with respect to x yields the change in flow dq through a small volume element $A \cdot dx$ where

$$dq = - \frac{kA}{\mu} \cdot \frac{d^2P}{dx^2} \cdot dx \quad (I.1)$$

This relation indicates that the change in flow along the sample - $(\frac{dq}{dx})$ - is directly proportional to the change in gradient $[\frac{d^2P}{(dx^2)}]$ along the sample length.



XBL 8011-3967

Fig. I.1 Schematic of a porous cylindrical rock sample subjected to hydrostatic compression.

The mass of fluid (M) stored in the differential volume $A \cdot dx$ is

$$M = (n\rho) (A dx) , \tag{I.2}$$

where the porosity n is the net pore volume V_p divided by the total sample volume V and ρ is fluid density. Assuming changes in fluid mass (dM) occur only as a result of application of a pressure pulse in the upstream reservoir

$$dM = (\rho dn + n d\rho) A dx , \tag{I.3}$$

where changes in porosity dn are due to rock compressibility β_R and changes in fluid density $d\rho$ are due to fluid compressibility β . The equation of continuity of mass requires that $\rho V = \text{constant}$ where the total sample volume V is the sum of the pore volume V_p plus the volume of solids V_R and the volumes of the upstream and downstream reservoirs V_U and V_D respectively. Total differentiation of this relationship with respect to pressure P yields

$$\frac{d\rho V}{dP} = \frac{\rho dV}{dP} + \frac{V d\rho}{dP} = 0 \quad (\text{I.4})$$

or

$$\frac{d\rho V}{dP} = \rho d(V_p + V_R + V_U + V_D) + (V_p + V_R + V_U + V_D)d\rho = 0 \quad (\text{I.5})$$

Reservoir volumes (V_U and V_D) and the total volume of solids (V_R) are considered constant throughout a pressure pulse test. Thus the change in total volume, as a function of pressure, is only dependent upon change in the pore volume (dV_p) and upon changes in fluid density ($d\rho$).

Expressing $d\rho = -\frac{1}{\beta} \frac{dV}{V}$ in terms of pore fluid density ρ yields:

$$d\rho = \frac{1}{\beta} \frac{d\rho}{\rho} ; \quad (\text{I.6})$$

thus $\rho\beta dP = d\rho$. (I.7)

Substituting $\rho\beta dP$ for $d\rho$ in equation I.3 and rewriting in terms of the total volume of fluid storage S (rather than mass of fluid storage M) yields

$$S = Adx(dn + n\beta dP) \quad (\text{I.8})$$

In this experiment porosity varies strictly as a function of variations in fluid pressure (as controlled by rock compressibility) thus according to Brace et al. (1968),

$$dn = (-n\beta_s dP - dn_e) \quad (\text{I.9})$$

where β_s is the solid grain compressibility and dn_e is the change in porosity due to a change in external pressure. Walsh (1965) has shown that

$$dn_e = (\beta_s - \beta_{eff}) dP \quad (I.10)$$

where β_{eff} is the effective compressibility of a jacketed rock sample.

Thus the storage S is

$$S = Adx[-n\beta_s dP - (\beta_s - \beta_{eff})dP] + A dx[n\beta dP] \quad (I.11)$$

and the total change in storage dS in time dt is

$$dS = A dx([-n\beta_s - \beta_s + \beta_{eff}] \frac{dP}{dt} + n\beta \frac{dP}{dt}) dt . \quad (I.12)$$

The net change in storage ds during time dt must equal the net change in flow $(-dq)$. Thus from (I.12) and (I.1)

$$\frac{k}{\mu} A \frac{\partial^2 P}{\partial x^2} dt dx = A dx (-n\beta_s - \beta_s - \beta_{eff} + n\beta) \frac{\partial P}{\partial t} dt \quad (I.13)$$

or

$$\frac{\partial^2 P}{\partial x^2} = \frac{\mu}{k} [-\beta_s (1 + n) + \beta_{eff} + \beta_n] \frac{\partial P}{\partial t} .$$

Equation (I.13) can be expressed in the form

$$\frac{\partial^2 P}{\partial x^2} = a^2 \frac{\partial P}{\partial t} ; \quad a^2 = \frac{\mu}{k} [\beta_s (1 + n) + \beta_{eff} + \beta_n] \quad (I.14)$$

where $t > 0$ and $0 < x < L$.

This equation is the linear parabolic diffusivity equation which describes the transient flow of a compressible fluid through a porous compressible rock

sample. The a^2 term contains terms for fluid properties (viscosity and compressibility). The boundary conditions shown in Fig. I.2 are derived as follows. Assuming a constant upstream reservoir volume, a decrease in fluid pressure within the reservoir is equivalent to a decrease in fluid mass (dM_U) within the reservoir (due to the fluid compressibility β) where

$$dM_U = M_U \beta dP \quad (I.15)$$

from Eq. (I.8). As the pressure decays the mass flow rate of fluid ($q\rho$) through the sample in time dt , according to Darcy's law, is

$$-q\rho = \frac{dM}{dt} = \rho \frac{k}{\mu} A \frac{dP}{dx} . \quad (I.16)$$

Replacing dM in (I.16) with the expression for dM_U from (I.15) yields

$$\beta V_U \frac{\partial P}{\partial t} = \frac{k}{\mu} A \frac{\partial P}{\partial x} \quad (I.17)$$

or

$$\frac{\partial P}{\partial x} = \lambda_U \frac{\partial P}{\partial t} , \quad \lambda_U = \frac{\beta \mu V_U}{Ak} \quad (I.18)$$

for $t > 0$ and $x = 0$.

A similar procedure yields the boundary conditions at the downstream reservoir:

$$\frac{\partial P}{\partial x} = \lambda_D \frac{\partial P}{\partial t} , \quad \lambda_D = \frac{-\beta \mu V_D}{Ak} . \quad (I.19)$$

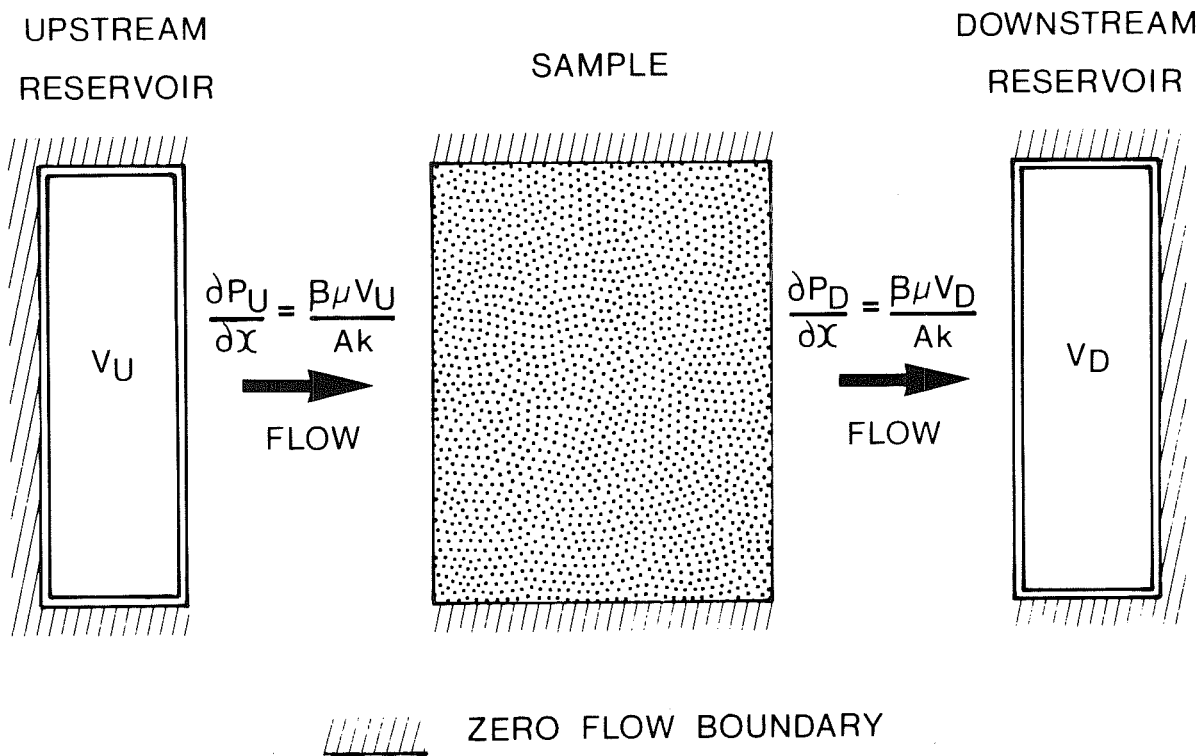
The initial conditions are defined by

$$P(0, 0) = P_0 \quad \text{and} \quad P(x, 0) \quad \text{for} \quad 0 < x \leq L \quad (I.20)$$

where $P_0 = \Delta P + P_i$

and the final condition is

$$P(x, \infty) = P_i + \frac{\Delta P V_U}{V_U + V_D + nV_R} = P_E . \quad (I.21)$$



XBL 8011-3968

Fig. I.2 Boundary conditions for a porous cylindrical sample.

Thus an instantaneous pressure increase ΔP above the ambient pore pressure P_i is assumed. The final equalized pressure (P_E) is equal to the ambient pressure (P_i) plus ΔP , all multiplied by the ratio of upstream reservoir volume to total fluid volume in the system.

Significant assumptions made in developing the above equations are:

1. Rock sample is unfractured, homogeneous and isotropic.
2. Fluid properties (compressibility and viscosity) and rock properties (permeability and compressibility) are constant throughout the test. This requires isothermal conditions and small pressure pulses (ΔP).
3. External dimensions of the rock sample are considered constant throughout the test.
4. The pressure pulse results from an instantaneous increase of pressure within the upstream reservoir.
5. Reservoir dimensions remain constant throughout the test.

A modification of the upstream boundary condition is proposed in a later section which will result in removal of the assumption of constant upstream reservoir dimensions (assumption 5).

I.2 Porous Cylindrical Sample Containing a Single Fracture

The derivation of the equation describing a laboratory pulse test performed on a rock of low permeability, containing a single fracture, is similar to the derivation of the equation for the porous sample discussed in the previous section. However, in this discussion it is assumed that the matrix permeability is sufficiently low such that the volume of water flowing through the rock matrix is negligible when compared to the volume of water

flowing through the fracture. Thus, the laminar, parallel-plate flow law is used instead of Darcy's law and the effects of fracture stiffness on permeability and porosity must be considered. A schematic of the rock sample with a single fracture is shown in Fig. I.3. Following the approach outlined in the previous section and using the basic principles of Chapter 2, we find the rate fluid flow through the sample is

$$q = - \frac{k_f w 2b}{\mu} \frac{dP}{dx} \quad (I.22)$$

where $k_f = \frac{(2b)^2}{12}$

is the fracture permeability expressed in terms of fracture aperture $2b$, and w = fracture width. Differentiating Eq. (I.22) with respect to x yields the change in flow through a small volume element $A dx$:

$$dq = - \frac{k_f w 2b}{\mu} \frac{d^2 P}{dx^2} dx \quad (I.23)$$

The net storage in the differential volume is controlled by fluid and rock compressibility and fracture stiffness:

$$S = A dx [(n_f + n) \beta dP + dn + dn_f] \quad (I.24)$$

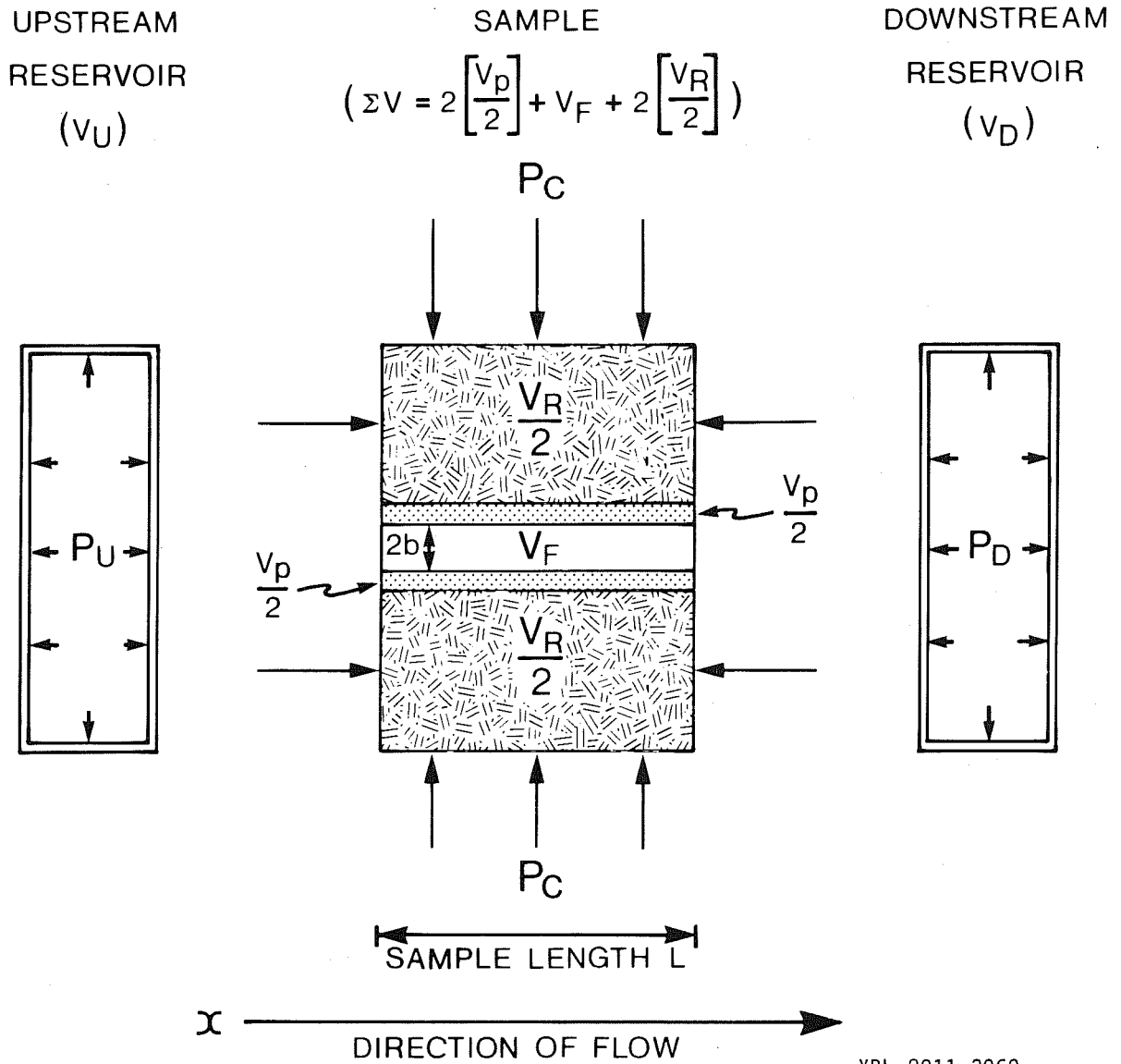
which is similar to Eq. (I.8). However, here an additional term is required to portray both changes in pore volume and fracture volume. Thus

$$S = A dx [(-n \beta_S - \beta_S + \beta_{eff}) dP + dn_f + \beta (n + n_f) dP] \quad (I.25)$$

$$n = \text{void porosity} = V_p/V,$$

$$n_f = \text{fracture porosity} = \frac{V_f}{V} = \frac{2b \times A_f}{V} \quad ,$$

where A_f is the surface area of fracture. In this equation the first term represents fluid storage due to compression of the solid matrix, the



XBL 8011-3969

Fig. I.3 Schematic of a porous cylindrical rock sample containing a single fracture and subjected to hydrostatic compression.

second term represents fluid storage due to fracture compression and the third term represents storage due to fluid compression. Again the net change in storage dS in the time dt must equal the net change in flow - dq during time dt . Thus from (I.1) and (I.25):

$$\frac{\partial^2 p}{\partial x^2} = \frac{\mu}{k_f} \left[-n \beta_s \frac{\partial p}{\partial t} + n \beta \frac{\partial p}{\partial t} + \frac{dn_f}{dt} + n_f \beta \frac{\partial p}{\partial t} - (\beta_s - \beta_{eff}) \frac{\partial p}{\partial t} \right],$$

or

$$\frac{\partial^2 p}{\partial x^2} = \frac{\mu}{k_f} \left\{ [(-\beta_s(1+n) + \beta_{eff} + \beta(n+n_f)) \frac{\partial p}{\partial t} + \frac{dn_f}{dt}] \right\}. \quad (I.26)$$

Considering variations of fracture porosity with time ($\frac{dn_f}{dt}$) requires the additional assumption that no shearing exists along the fracture plane. Thus fracture deformation is strictly a variation of fracture aperture $2b$. Fracture aperture varies as a function of the outward normal force F such that an increase in outward normal force (equivalent to an increase in pore pressure) causes an increase in fracture aperture. Thus

$$K_n = \frac{dF}{d(2b)}, \quad (I.27)$$

where K_n is the fracture stiffness (change in normal stress per unit normal displacement). Thus if the surface area of the fracture is A_f (equal to fracture width W times core length L),

$$d(2b) = \frac{A_f dP}{K_n} = \frac{WL dP}{K_n}. \quad (I.28)$$

$$\text{Rewriting } n_f \text{ as } \frac{W \cdot 2b \cdot L}{V}, \quad (I.29)$$

$$\frac{dn_f}{dt} = \frac{Wd(2b)}{A dt}, \quad (I.29)$$

which, when substituted in (I.28), yields

$$\frac{dn_f}{dt} = \frac{W}{A} \left(\frac{WL}{K_n} \frac{dP}{dt} \right) \quad \text{or} \quad \frac{dn_f}{dt} = \frac{4L}{\pi k_n} \frac{dP}{dt} \quad (\text{I.30})$$

if the fracture width W is equivalent to the core diameter. Thus substituting (I.26) into (I.22) yields an equation of form

$$\frac{\partial^2 P}{\partial x^2} = a^2 \frac{\partial P}{\partial t} \quad (\text{I.31})$$

where
$$a^2 = \frac{\mu}{k_f} \left[\frac{4L}{\pi K_n} + \beta(n_f + n) - \beta_s(n + 1) + \beta_{\text{eff}} \right]$$

and
$$k_f = \frac{(2b)^2}{12} .$$

The boundary, initial and final conditions are similar to those derived for the porous sample (Eqs. (I.18) and (I.19)). However, the parallel-plate, laminar flow law is used in deriving the boundary conditions (Fig. I.4).

Thus:

$$\frac{\partial P}{\partial x} = \lambda_U \frac{\partial P}{\partial t} \quad \text{where} \quad \lambda_U = \frac{\beta \mu V_U}{W 2 b k_f} \quad (\text{I.32})$$

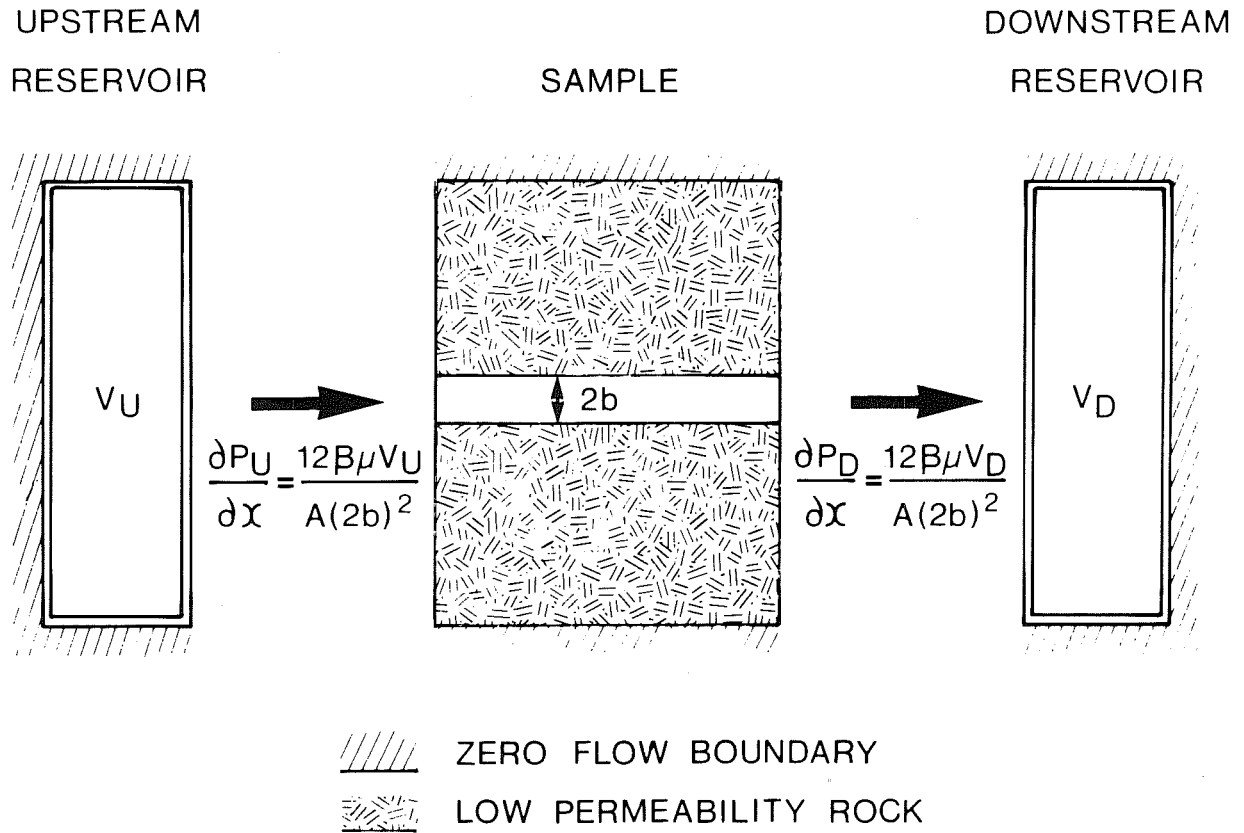
$$t > 0 \text{ and } x = 0$$

$$\frac{\partial P}{\partial x} = \lambda_D \frac{\partial P}{\partial t} \quad \text{where} \quad \lambda_D = \frac{\beta \mu V_D}{W 2 b k_f} \quad (\text{I.33})$$

$$t > 0 \text{ and } x = L$$

and
$$k_f = \frac{(2b)^2}{12} .$$

The assumptions made in the development of Eq. (I.31) are the same as those outlined in the previous section except that the first assumption of section I.1 is modified to read:



XBL 8011-3970

Fig. I.4 Boundary conditions for a porous cylindrical sample containing a single fracture.

1. Rock sample contains a single fracture continuous across the core width and the matrix is effectively impermeable (when compared to the permeability of the fracture). The fracture is also parallel to, and centered on, the core axis.

I.3 Modification of Upstream Boundary Conditions to Include Packer Compliance Effects in a Simulated Borehole

This section proposes a re-derivation of the upstream boundary conditions to include a compliance term which allows removal of part of assumption 5 (upstream reservoir volume is constant). In a simplistic manner we can represent compliance in the upstream reservoir (assumed to be solely the result of packer movement within the simulated borehole) by a piston held in place by a spring (Fig. 2.2) with stiffness C . The complex combination of the effects of packer friction in the borehole, packer shape, packer materials (stiffness) and packer expansion techniques (allowing different variations in reservoir volume during pressure pulse application) are represented by the spring coefficient C . Thus, if the system is in equilibrium at a specified internal pressure, a decrease in pressure due to flow through the sample (pulse decay) will cause displacement of the piston (with area A_p) yielding a decrease in reservoir volume according to the relation

$$dV = A_p \cdot dx = A_p \frac{dF}{C} = \frac{(A_p)^2 dP}{C} \quad (I.34)$$

where $dF = Cdx$.

The net volume change (dV) within the reservoir is therefore governed by the packer compliance and fluid compressibility where

$$dV = \beta V dP + \frac{(A_p)^2}{C} dP \quad (I.35)$$

The decrease in reservoir volume is equivalent to the outflow of fluid through the sample where

$$\frac{\partial V}{\partial t} = \frac{kA_p}{\mu} \frac{\partial P}{\partial x} = \beta V_U \frac{\partial P_U}{\partial t} + \frac{(A_p)^2 \partial P_U}{C \partial t} \quad (I.36)$$

thus returning to the form of the previous boundary conditions

$$\frac{\partial P}{\partial x} = \lambda_U \frac{\partial P_U}{\partial t} ; \quad \lambda_U = \frac{\mu}{kA} \left(\beta V_U + \frac{A_p^2}{C} \right) \quad (I.37)$$

where permeability k may be either porous media (k) or fractured rock

($k_f = \frac{(2b)^2}{12}$). Unfortunately, it is rather difficult to isolate and calculate the various components of the compliance factor C . However, this form of the boundary condition will be used in later computer simulations of the test set-up to provide an estimate of the relative effect of various packer compliances on pressure-time decay curves.

APPENDIX II
TEST EQUIPMENT AND PROCEDURES

II. 1 Experimental Apparatus

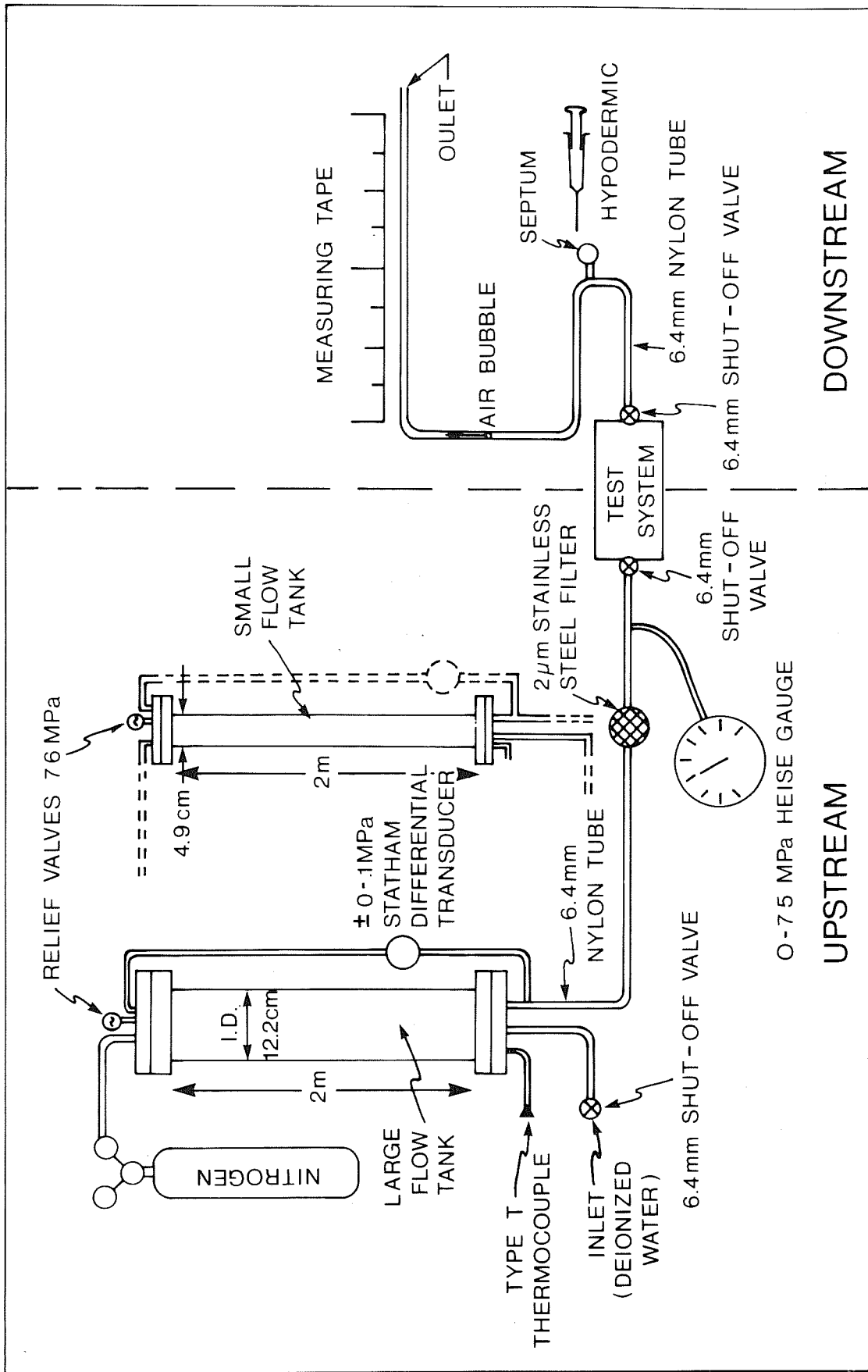
This section presents and discusses the details of the test equipment shown in Fig. 3.1.

II. 1.1. Pressure Application and Flow Monitoring

A detailed schematic of the pressure application and flow monitoring component is shown in Fig. II. 1. Fluid pressure is generated within the system by applying the desired internal pressure to the flow tank using compressed nitrogen. During steady-state flow tests the flow of water through the sample is calculated from measurements of the change in water level in the flow tank over a specified time period. The drop in water level (monitored by a differential pressure transducer) corresponds to a decrease in volume of water in the tank. Two tanks of different sizes were constructed so as to allow flexibility in choice of flow measurement times (depending upon the permeability of the sample to be tested).

A thermocouple is inserted into the base of the tank to monitor temperature variations in the water leaving the tank. Downstream of the flow tank a 2 μ m sintered stainless steel filter is positioned to remove particulate matter from the water. The filter is installed to aid in preventing permeability variations which could result from plugging of the sample pores. The 0 - 6.9 MPa Heise gauge is used for in-line calibration of the two absolute transducers located on each side of the sample cell (Fig. 3.1).

An alternative technique used for measurement of low flow rates requires a calibrated tube of uniform inside diameter attached to the outlet at the downstream reservoir. An air bubble is injected, with a hypodermic, through a septum into the tube and the time for the bubble to travel a specified



XBL 8011-3971

Fig. II.1 Schematic of the flow monitoring and pressure application component.

distance is measured. Flow rates may be calculated from the bubble velocity and tube calibration.

II.1.2. Simulated Borehole and Borehole Seals

A detailed schematic of the simulated borehole system and its five major subcomponents is shown in Fig. II.2.

The simulated borehole is a 7 m long, 6.4 mm thick, steel tube with inside diameter of 76 mm. The tube may be separated at the middle, allowing different equipment configurations, by disconnecting the flanges attached to each section of tube. One tube section has two flanges so that a solid plate may be bolted on one end to seal the end of the tube. The other tube section has only the connecting flange required to bolt the two tube sections together.

A steel collar is attached to the tube to provide extra strength where the holes that house the thermocouple, piston displacement screw, "feed through" and connection to the sample cell penetrate the borehole. The piston displacement screw is used to generate a pressure pulse within the borehole and is shown schematically in Fig. II.2. A displacement of 2 cc is created for each 360° turn on the handle, allowing for precise pressure pulse generation. The thermocouple is positioned in the tube so as to monitor temperature changes that may occur in the tube during pulse generation. The "feed through" (Fig. II.2) is a 3-conductor seal that allows strain signals generated within the borehole to be transmitted along the conductors to the data acquisition system. The connections to the sample cell component consist of a 13-mm-diameter stainless steel tube of 0.89 mm wall thickness, 2 ball valves, one shut-off valve, a 60 μ m sintered stainless steel filter, a thermocouple and a 0 - 3.4 MPa Shaevitz absolute pressure transducer connected

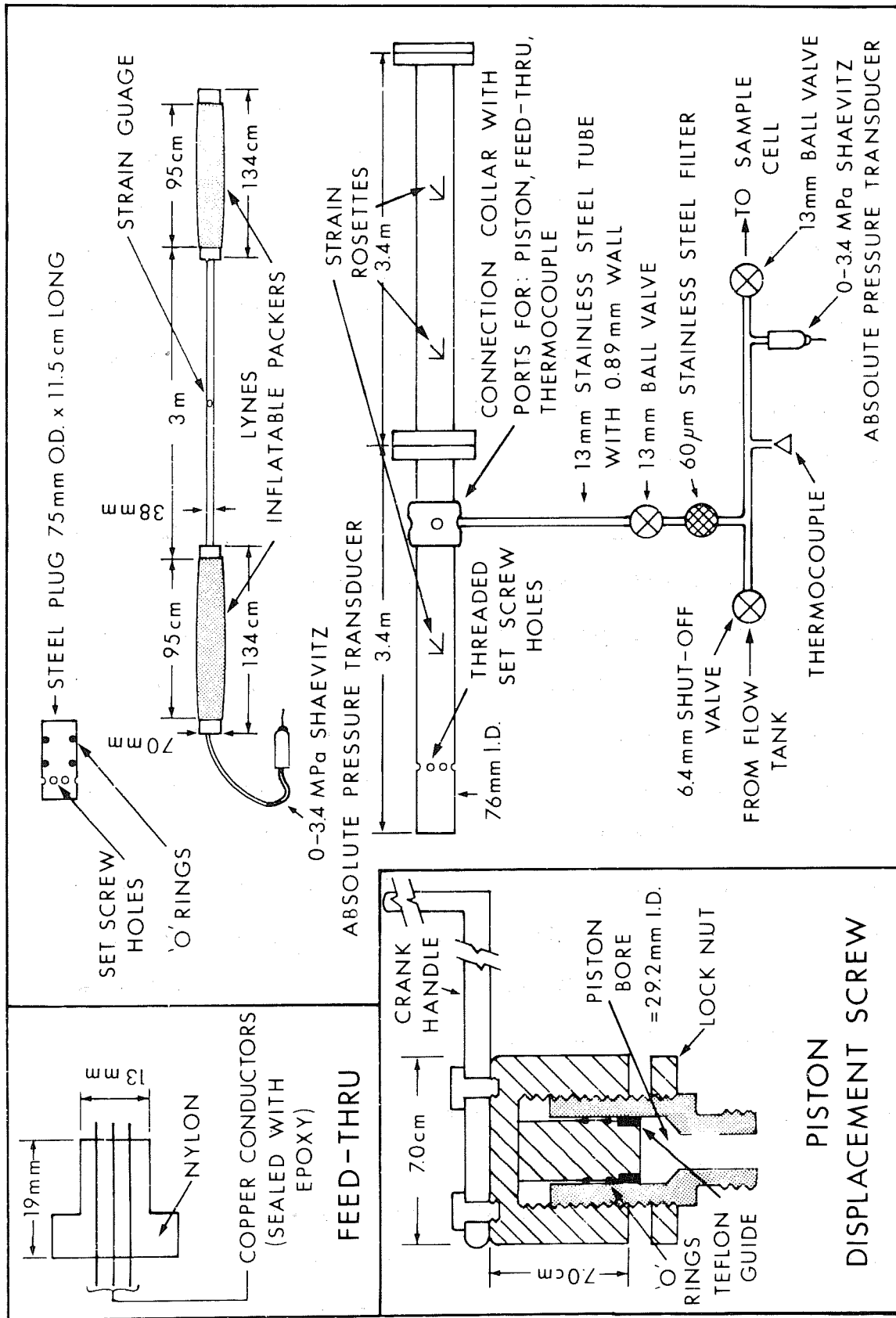


Fig. II.2 Schematic of the simulated borehole and borehole seals. XBL 8011-3972

in the configuration shown in Fig. II.2. The ball valves allow the borehole to be shut off from the sample cell without introducing the volume change effects usually caused by standard shut-off valves. Volume changes caused by closure of a standard valve can cause appreciable changes in fluid pressure. The relatively large opening 60 μm filter is positioned to prevent particulate matter from the borehole from entering the sample without attenuating the pressure pulse. The thermocouple monitors the temperature of the water before it enters the sample cell while the pressure transducer monitors the pressure upstream of the rock sample.

Borehole seals are of two types: Standard NX Lynes inflatable packers and a 115 mm x 76 mm diameter steel plug. Two packers (separated by a 3 m long x 2.54 mm diameter rod) may be inserted into the full-length borehole and positioned with centers at the external strain gauge positions. The packers may be inflated with air or water and the inflation pressure (applied by compressed nitrogen) is monitored by a 0 - 6.9 MPa Shaevitz absolute pressure transducer. Alternatively, the steel plug may be inserted into the borehole segment that holds the connection collar and the plug is kept in place by 6 Allen screws set in holes drilled in the borehole. The stiff, non-compliant test interval is simulated by the steel plug while the packers provide a more compliant test cavity.

Strain gauges have been applied externally to the borehole and on the bar which joins the two packers. On the borehole the strain rosettes (each gauge is 6.4 mm long) are positioned (near the center of the simulated cavity and at the packer centers), to measure the circumferential and axial strains and strains at 45° to the tube axis. A 6.4 mm strain gauge mounted on the

bar (parallel to the bar axis) is used to monitor the extension and contraction of the steel bar between the packers. These gauges will be used to estimate the magnitude of volume change effects that may occur in the borehole cavity due to packer separation and borehole deformation.

II.1.3 Hydrostatic Sample Cell

The hydrostatic sample cell (a modified Hoek-Franklin cell) and associated equipment is shown in the schematic on Fig. II.3. In this discussion the equipment for applying a confining pressure to the sample will be labeled the oil system while the equipment containing water will be called the water system. The oil system consists of the following:

- i) Sample cell to hold a cylindrical sample 11.5 cm long by 5.4 cm in diameter.
- ii) Hydraulic pump to provide a confining pressure up to 35 MPa.
- iii) Heise gauge (0 - 52 MPa) and Norwood absolute pressure transducer (0 - 52 MPa) to monitor variations in confining pressure.

A detailed sketch of the cell is shown in Fig. II. 3. Axial pressure is applied by a single piston with area calculated to provide the same axial and radial pressures. The radial pressure is transmitted through a urethane sleeve. The water pressures are distributed evenly over the ends of the sample by sintered stainless steel discs with openings of 40 μm . As shown in Fig. II.3 both end caps may be removed from the cell for sample insertion and removal of the cell component from the system without requiring deairing of the complete test set-up prior to resuming operations.

II.1.4 Downstream Reservoir

The downstream reservoir is a steel tank with inlet, outlet and dimensions as shown in Fig. II.4. A Shaevitz 0 - 3.4 MPa absolute pressure transducer is located near the tank to monitor fluid pressures downstream from the sample.

II.1.5 Data Acquisition System

The data acquisition system is shown schematically in Fig. II.5. The Fluke 2240-A multi-channel data logger reads the following sensor signals:

- i) voltage from pressure transducers and power supplies
- ii) temperature from the thermocouples

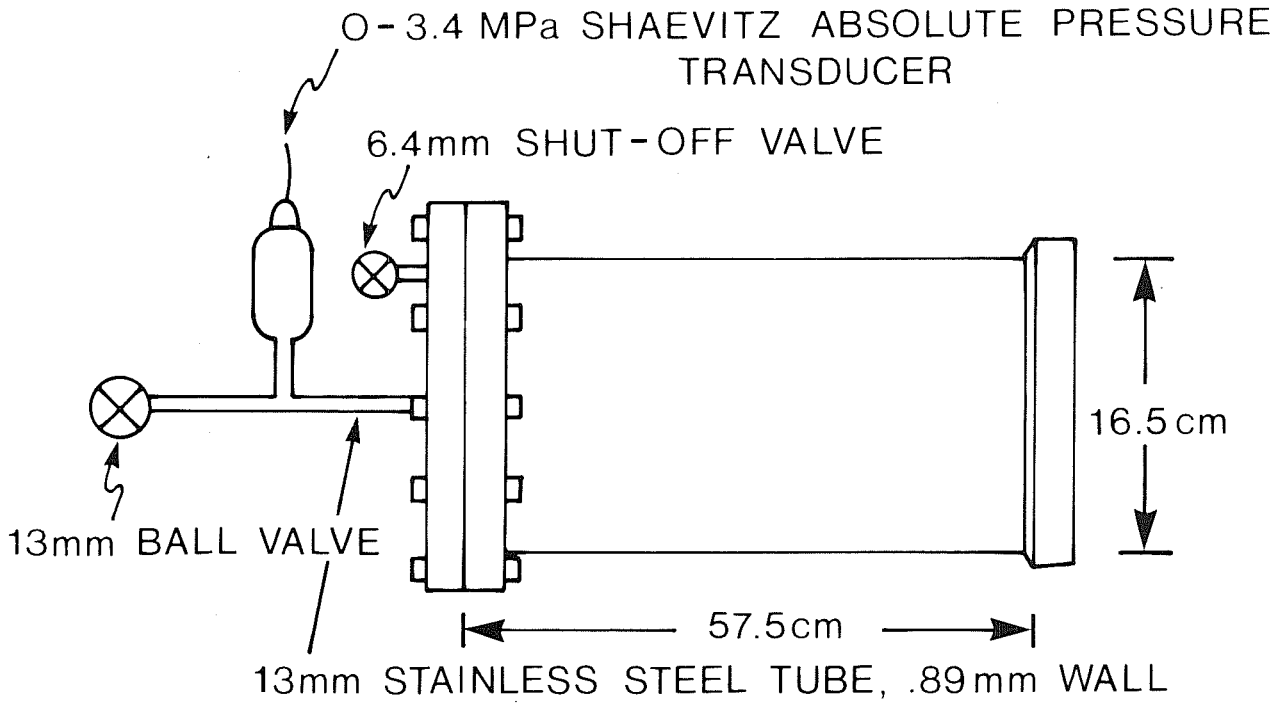
This data is printed and punch-coded by an ASCII teletype connected directly to the logger. Strain gauge data are read manually from a Budd decade box and entered on the output using the teletype keyboard. Bubble velocities and additional comments are also entered as required using the teletype keyboard. A visual display of individual sensor outputs is obtained on chart records from two 2-pen chart recorders.

II.2 Experimental Procedures

This section discusses the details of procedures used in permeability determinations (using steady-state and pressure pulse techniques), equipment calibration and sample preparation.

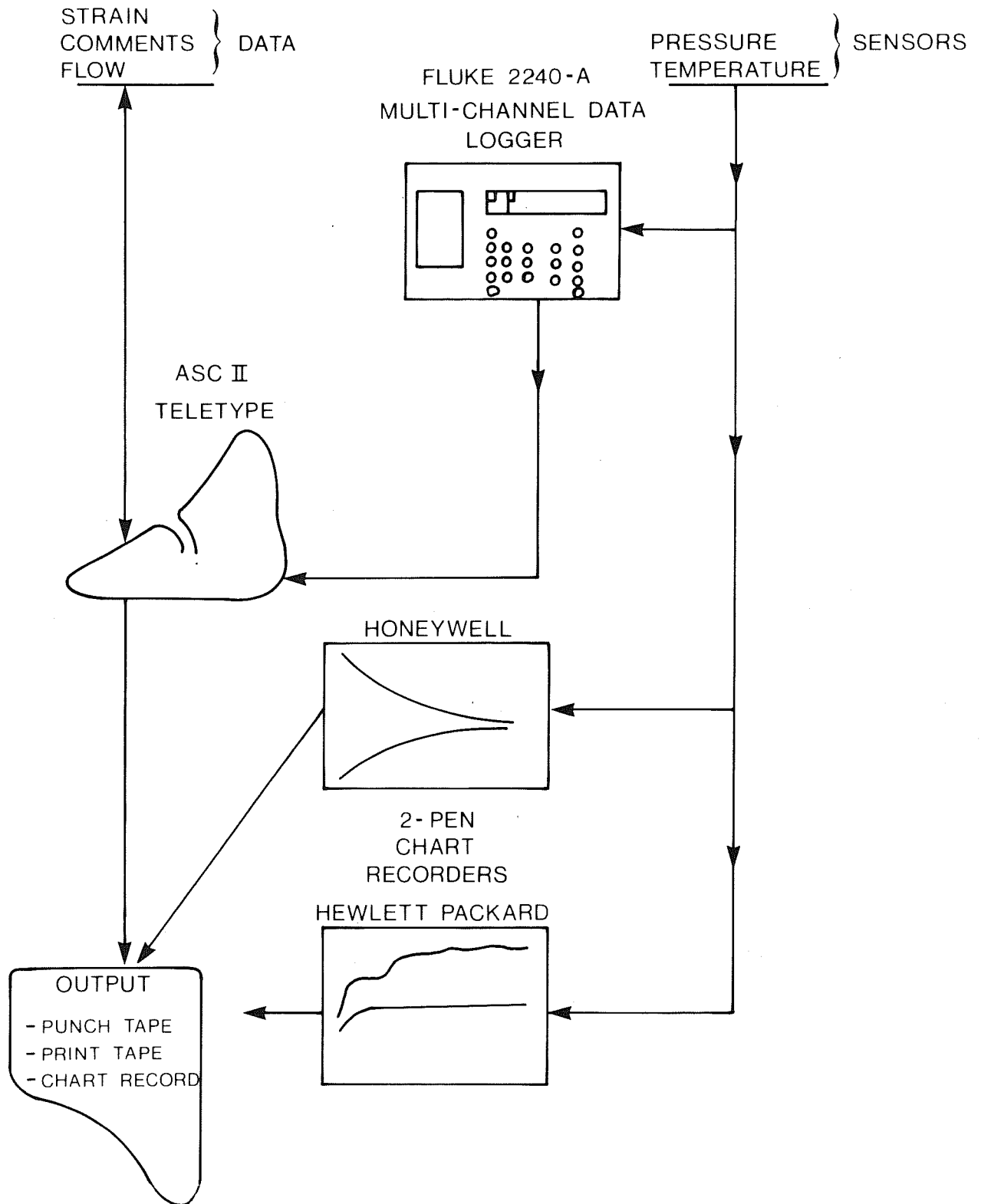
II.2.1 Equipment Calibration

Equipment which must be calibrated includes thermocouples, pressure transducers, flow tanks, bubble line and reservoir volumes. Strain gauges are factory calibrated and only a zero balance is required prior to each test. The Budd decade strain readout box used in this set-up provides a



XBL 8011-3974

Fig. II.4 Schematic of the downstream reservoir.



XBL 8011-3975

Fig. II.5 Schematic of the data acquisition system.

resolution of strains on the order of 1μ in/in.

Thermocouples are calibrated to determine the accuracy of the absolute temperature reading obtained from a single thermocouple and to compare differences between readings obtained from different thermocouples. Type T (copper - Constantan) thermocouples are used exclusively. The thermocouple generates a signal which is converted by the data logger to temperature in $^{\circ}\text{C}$ with a resolution of 0.1°C . All thermocouples used in the test set-up are calibrated simultaneously by inserting them into a well-stirred oil bath sitting on a hot plate. The oil bath temperature is varied by adjusting the heat of the hot plate. Temperature variations are monitored with a thermometer with 0.1°C graduations and with the thermocouple outputs displayed on the data logger. Several temperatures around room temperature (24°C) are checked so that the thermocouples are calibrated over a range of possible test temperatures. Calibration results indicate that absolute temperature readings may be read with an accuracy of $\pm 0.1^{\circ}\text{C}$. Readings obtained from two thermocouples at the same temperature agree in all cases. Thus, although the thermocouple readings differ up to 0.1°C from thermometer readings, all thermocouples yield the same reading at specified temperature.

Pressure transducers are calibrated against a Heise gauge or dead weight tester in the following manner:

1. The transducer is connected to a pressurizing system (compressed air or hydraulic dead weight tester) and voltage signals compared to gauge readings or dead weight tester weights.
2. Input power is monitored to check for variations in transducer signals resulting from variation in input power. Temperatures are

also monitored during calibration (although the transducers are temperature-compensated over the temperature range expected during use, 20°C to 25°C).

3. Pressure is increased to full scale and returned to zero to remove any stiffness in the transducer components.
4. At least 5 and generally 10 pressure settings are measured from 0 to the maximum desired pressure. Measurements are made during both the pressure increase and pressure decrease cycles.

Schaevitz absolute pressure transducers (0 - 3.4 MPa) used in the test set-up have been calibrated against an Ashcroft dead weight tester (accurate to ± 0.00069 MPa) and are regularly calibrated against an in-line 0 - 6.9 MPa Heise gauge with 0.0069 MPa graduations. The data logger is capable of reading voltage signals of 1 μ volt; thus, with a 5 volt output for 3.4 MPa (10 V input), a resolution of 0.00069 MPa is possible. Transducer errors due to non-linearity and hysteresis are in the order of $\pm 0.5\%$ of the full range output of the transducers. The maximum pressure changes generated during a particular test are 0.34 MPa thus an accuracy of ± 0.0017 MPa is expected. The transducers can be calibrated to this degree of accuracy by the dead weight tester. The Heise gauge can be used to calibrate the transducers to an accuracy of ± 0.0034 MPa. Thus pressure variations of 0.0034 MPa $\pm 0.5\%$ may be resolved. Calibration of the 0 to 6.9 MPa Schaevitz transducer used to monitor packer pressure yields similar results as the calibration is dependent upon the sensitivity of the Heise gauge.

The Statham differential transducer (± 0.1 MPa) is calibrated against a 0 to 0.1 Heise gauge with 6.9×10^{-5} MPa graduation. For a 10-volt input

a full scale output of 10 mV is obtained; thus the data logger allows resolution of 6.7×10^{-6} MPa. Transducer calibration against the Heise gauge indicates a maximum error of $\pm 1\%$ due to nonlinearity and hysteresis. This transducer is used for two purposes. During steady-state flow tests the unit is used to monitor water level change in the flow tank and the transducer is recalibrated to yield ml/volt. During transient tests the unit is used to check that the pressure difference across the sample is zero. The zero shift of the transducer (due to hysteresis and thermal effects) is minimal; thus the zero check is considered to be accurate.

The Norwood absolute transducer (0 to 52 MPa) is calibrated against a Heise gauge with graduations of 0.069 MPa. For an 11-volt input a full-scale output of 75 mV is obtained thus the data logger allows resolution of 0.00069 MPa. Transducer calibration against the Heise gauge indicates a maximum error due to non-linearity and hysteresis of $\pm 1\%$. This transducer is used to monitor the sample confining pressures of 34 MPa thus variations in confining pressure greater than 0.34 MPa may be accurately detected.

II.2.2 Flow Measurements

Flow tanks are calibrated by measuring the change in voltage output from the Stathan differential transducer for a specified volume of water removed from the tank. Calibrations indicate that over the operational pressure range (0 - 0.69 MPa) variations in tank volume and water compressibility are negligible. Temperature variations during calibration and testing are usually less than 2°C ; thus volume changes due to thermal expansion of the water and flow tanks are also negligible. Minimum measurable volume changes which are calculated to provide an accuracy of 1% are:

1. large tank - 543 ml
2. small tank - 122 ml

Thus, depending upon the desired time period of measurement, the associated flow rates accurate to 1% are:

1. large tank - 17.7 ml/min (30 min. test) to 532 ml/min (1 min. test)
2. small tank - 4.1 ml/min (30 min. test) to 122 ml/min (1 min. test)

The bubble line is calibrated by measuring the outflow from the tube during the time required for a specified distance of bubble travel. The accuracy of flow measurement depends upon the accuracy of the measurement of bubble travel (assuming negligible temperature and flow variations during the measurement period). A distance of bubble travel of 15 cm can be measured with an accuracy of $\pm 1\%$; thus, using a 1/4" nylon tube, the minimum measurable volume is 1.6 ml, and the minimum accurately measurable flow rate is 1.6 ml for a 1 min test and 0.05 ml/min for a 30 min test.

II.2.3 Sample Preparation

Samples are cored to the correct diameter using an open back diamond bit, then cut with a radial arm diamond saw. Water rather than oil is used in both cutting operations to reduce sample contamination. After cutting, samples are clamped in a vise for grinding both ends parallel. The vise holds the core axis perpendicular to both the faces to be ground and the grinding wheel. Again, water is used in the cutting operation. Sample lengths and diameters are measured with a vernier caliper. Parallelism of sample ends is measured by placing the core on a level, finely ground granite slab (core axis upright). A vertical gauge is placed so as to monitor the change in core height (at the core edge) as the core is rotated on the slab.

The deviation of the ends from parallel is expressed as the maximum deviation of the dial gauge.

Roughness of sample ends is measured as the maximum deviation of the dial gauge as it is moved about the end of the core while the core is held stationary. Perpendicularity is estimated by measuring the average distance between the core side (at the top of the core) and a set square placed on the granite slab (the set-square touches the core side at the core base). The core is kept between handling periods by storage in water bath. Phenol is added to the water to inhibit bacterial growth which may plug sample pores.

II.2.4 Steady-State Permeability Determinations

The steady-state permeability determination technique used in this experiment consists of measurement of the steady-state flow rate of water through a sample subjected to a known pressure gradient. A step-by-step procedure is outlined below:

1. Place prepared sample in cell and apply desired confining pressure.
2. Flush the sample and system with CO₂.
3. Flush the sample and system with deionized water (from the flow tank) and ensure by-pass is closed after completion of flushing.
4. Start data recording sequence on data logger/teletype and start chart record of flow tank level, upstream reservoir pressure and confining pressure.
5. Adjust upstream pressure by adjusting flow tank pressure (using compressed nitrogen bottle).
6. Observe data output until a sufficient period of steady pressure and steady flow is obtained.

7. Estimate flow frequently using the flow tank and/or bubble line data during the steady-state period of the test.
8. Run several tests at different confining pressures and different upstream pressures.

Points in the above procedure which should be expanded are references to CO₂ flushing and sample preparation. CO₂ is used to aid in deairing the sample and system as any CO₂ not expelled during water flushing will be dissolved. Thus bubbles of highly compressible gas will not form in the fluid system. Deionized water is also used to minimize water degassing and chemical interaction with the sample. The sample (a 11-cm-long, 5.4-cm-diameter right cylinder), is prepared so that the ends are parallel and smooth to 0.01 cm according to the technique outlined in the previous section.

The above procedure generates the following data which is used in calculation of sample permeability according to Darcy's Law where

$$q = - \frac{k\gamma_T}{\mu_T} \frac{dp}{dx} \cdot A$$

q = measured flow rate

γ_T and μ_T = water properties at the test temperature (weight density and dynamic viscosity) determined from data tabulated by Weist (1975)

A = measured area of sample

dx = measured length of sample

dP = measured difference between upstream and downstream pressures.

II.2.5 Transient Pressure Pulse Determinations

Transient pressure pulse tests are performed on samples which have not been removed from the cell after steady-state testing according to the

following step-by-step procedure.

1. Adjust confining pressure to desired value, ensure bypass is open and close outlet after obtaining zero reading on sensors.
2. Start data acquisition and chart records of upstream pressure, downstream pressure, confining pressure and differential pressure across the cell.
3. Adjust the water pressure to the desired value using compressed nitrogen at the flow tank. Record strain measurements.
4. Calibrate upstream and downstream pressure transducers against the in-line Heise gauge over the range of pressure to be encountered in test.
5. Close the bypass valve.
6. Close valve upstream of the sample cell.
7. Adjust the desired pulse increment in the borehole using the piston displacement screw and monitoring the in-line Heise gauge. Record strain measurement.
8. Close valve leading to the flow tank.
9. Start test by opening the ball valve upstream of the sample cell.
10. Test is completed when the differential transducer indicates zero pressure gradient across the sample or when a specified minimum differential pressure is achieved. Record final strain measurement.
11. Further tests are conducted in the same manner for different pore pressure and borehole seal configurations. Each time the borehole seal is changed the upstream portion of the system is flushed with CO₂ and water as outlined previously.

The data output yields pressure-time data and temperature-time data which may be compared to pressure-time data generated by a numerical simulation of the theoretical problem described in Chapter 2.

APPENDIX III
SAMPLE DESCRIPTIONS

III.1 Berea Sandstone

Samples of Berea sandstone were cored from two sandstone blocks obtained from Cleveland Quarries, Ohio. The blocks measured 30 x 30 x 15 cm and were cut with the 15 cm face parallel to the bedding planes. The vendor of the blocks reported that the blocks had an approximate permeability difference of one order of magnitude.

Sample 2-B1 was cored from a sandstone block described as follows:

- uniform medium grained sandstone
- silica matrix
- homogeneous in appearance
- medium grey in color with faint bedding
- unfractured

The sample was cored parallel to the observed bedding to minimize permeability contrast along the sample. Sample ends are parallel to within 0.03 mm and perpendicular to within 2 mm. The roughness of the sample ends is 0.0075 mm. The sample is 11.529 cm in length and 5.412 cm in diameter.

Sample 13-B2 was cored from another sandstone block described as follows:

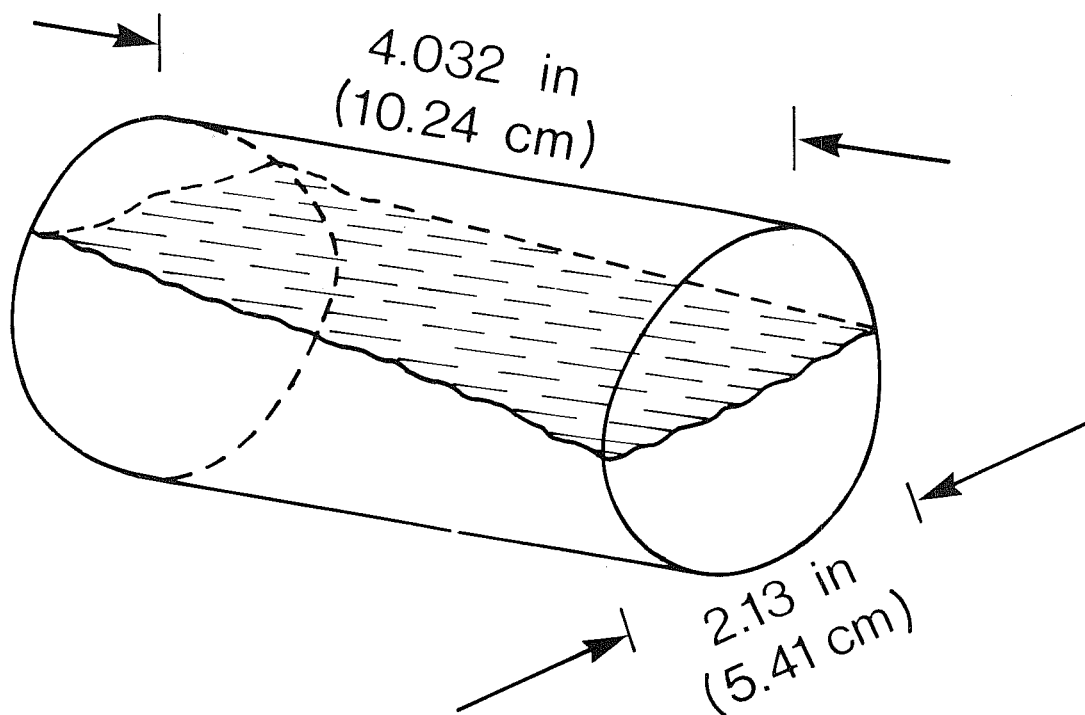
- fine to medium grained sandstone
- silica matrix
- reasonably homogenous in appearance
- grey-brown in color with distinct bedding
- unfractured

This sample was also cored parallel to the observed bedding planes. Sample ends were found to be parallel to 0.0064 mm and perpendicular to 0.0025 mm.

The roughness of the sample ends was found to be 0.025 mm. The sample is 11.440 cm in length and 5.41 cm in diameter.

III.2 Stripa Granite

The sample of Stripa Granite contains a single open fracture parallel to and approximately centered on the core axis (Fig. III.1). The core was cut and ground to provide parallel ends perpendicular to the core axis. The fracture was wedged open after the core was prepared and was found to be planar with a rough surface. A complete description of the mineralogic composition of the Stripa granite is given by Olkiewicz et al. (1978) and its mechanical properties are described by Swan (1978).



XBL 8011-3976

Fig. III.1 Sketch of Stripa granite sample.

